Analyst

ROYAL SOCIETY OF CHEMISTRY

MINIREVIEW

View Article Online
View Journal | View Issue

Cite this: *Analyst*, 2026, **151**, 1519

Recent advances in microneedle-based electrochemical biosensors for monitoring biomarkers in interstitial fluid

Renqiang Yuan, Xiaoxin Ma, Guda Zou, Guohuang Zhou, Jia Liu, Wei Li, Yixin Xu, Shao Su * and Lianhui Wang *

Microneedle (MN)-based electrochemical biosensors have emerged as a revolutionary technology for minimally invasive diagnostic applications and point-of-care (POC) testing of biomarker-rich interstitial fluid (ISF). Featuring painless skin penetration, rapid electrochemical response, high sensitivity, and seamless integration with portable/wireless devices, MN-based electrochemical biosensors offer distinct advantages over conventional invasive or lab-based assays. Therefore, this review comprehensively summarizes the recent advances in MN-based electrochemical biosensors. It begins by introducing the design strategies and unique advantages of different microneedle platforms for efficient ISF sampling. Subsequently, the review elaborates on the construction of MN-based electrochemical biosensors. Furthermore, the application progress of these biosensors for monitoring a wide range of biomarkers, including metabolites, hormones, electrolytes, nucleic acids and proteins, is systematically highlighted. Finally, the current challenges and future perspectives in this rapidly evolving field are discussed, outlining the development path toward next-generation MN-based electrochemical diagnostic devices.

Received 28th November 2025,
Accepted 5th February 2026

DOI: 10.1039/d5an01250c

rsc.li/analyst

1. Introduction

With the growing demand for personalized healthcare and health monitoring, the development of technologies capable of real-time, continuous, and minimally invasive monitoring of key physiological indicators has become a core challenge and cutting-edge direction in the field of biomedical engineering. Conventional *in vitro* diagnostics based on venous blood collection face significant limitations, including inherent invasiveness, reliance on clinical settings, and prolonged analytical timelines. These constraints prevent real-time biomarker monitoring and hinder their application in point-of-care testing (POCT) and personalized health management.[1–3] ISF has emerged as a highly promising alternative biofluid. As an extracellular reservoir in the dermis, ISF is rich in physiologically relevant biomarkers, such as metabolites, electrolytes, and hormones. Crucially, their concentrations in ISF exhibit a strong correlation with blood levels, establishing ISF as a valid and minimally invasive source for diagnostic information.[4–6] In contrast to blood testing, ISF-based biomarker detection eliminates invasive venipuncture, reduces needle-related infection risks, and avoids interference from blood cells, platelets or clotting cascades. Currently, conventional methods for efficiently extracting ISF face huge challenges including dermal confinement, poor accessibility, low extraction efficiency, bulky auxiliary instruments, complex processing flow, and high costs. Fortunately, the MN technology addresses these critical limitations through unique structural and functional merits that enable minimally invasive direct ISF extraction and real-time *in situ* sensing, unlocking ISF-based diagnostic potential.[7–9] Owing to these advantages, microneedles (MNs) have emerged as a sampling tool to construct a core system for biomarker monitoring,[10] compared with repeated venipunctures. Meanwhile, MNs have also been functioning as a well-established platform for tunable intradermal delivery[11] and wearable systems (*e.g.*, optoelectronic devices[12]). Based on the dual sensing–delivery functionalities, the integrated closed-loop diagnosis and therapeutic system will be promising for simultaneous biomarker monitoring and drug administration.

Recently, MN-based biosensors coupling minimally invasive percutaneous microneedles and advanced sensing elements represent a transformative paradigm in biosensing.[13–15] The versatility of the MN biosensing platform is demonstrated by its successful integration with a diverse range of biosensing modalities, including fluorescence, colorimetry, surface-enhanced Raman scattering, and electrochemistry.[16–18] Its principal advantages include (1) direct, painless access to

State Key Laboratory of Flexible Electronics (LoFE) & Jiangsu Key Laboratory of Smart Biomaterials and Theranostic Technology, Institute of Advanced Materials (IAM), Nanjing University of Posts and Telecommunications, 9 Wenyuan Road, Nanjing 210023, People's Republic of China. E-mail: iamssu@njupt.edu.cn, iamlhwang@njupt.edu.cn

in situ ISF, eliminating the need for venipuncture; (2) capability for real-time, continuous monitoring of dynamic physiological processes; and (3) user-friendly suitability for patient-centric and point-of-care applications, potentially enabling self-administration and facilitating decentralized healthcare.[19–21] Among them, MN-based electrochemical biosensors have gradually emerged as some of the most prominent and technologically compelling platforms for advanced POCT. Their exceptional advantages for real-time, continuous, and decentralized health monitoring lie in high sensitivity and selectivity, direct and rapid signal transduction, inherent ease of miniaturization and integration into wearable formats. A quintessential and commercially mature example is the continuous glucose monitoring (CGM) system. The CGM system employs enzyme-functionalized microneedles to electrochemically detect glucose in the ISF, demonstrating a high correlation with blood levels and revolutionizing diabetes management. This paradigm underscores the powerful synergy between electrochemical biosensing technology and MN technology for reliable, patient-friendly, and integrated POCT, solidifying its leading role in the evolution of personalized diagnostics.[22]

Nowadays, significant advances in MN-based electrochemical biosensors are being realized. In this review, we aim to provide a comprehensive overview of recent progress in this field through the following aspects: (1) to systematically summarize the structural designs of microneedles for efficient and reliable interstitial fluid sampling; (2) to elaborate on the construction strategies of MN-based electrochemical biosensors; (3) to highlight their expanding applications in monitoring diverse biomarkers. Furthermore, we provide insightful discussions on the integration of these microneedle-based electrochemical biosensing systems with wearable platforms for synchronous POC monitoring of multiple biomarkers. Finally, we critically discuss the remaining challenges and future perspectives, which will pave the way for transforming these promising technologies into practical clinical diagnostic tools.

2. Microneedle design for sampling ISF

To sample ISF efficiently, microneedles tailored for functional demands are designed into distinct types (Fig. 1), including solid MNs (SMNs), hollow MNs (hMNs), porous MNs (PMNs), and hydrogel MNs (HMNs). Each design category targets core challenges of ISF extraction, including minimally invasive access, efficient fluid collection, and compatibility with downstream detection, laying the foundation for practical point-of-care diagnostic applications.

2.1. Design of SMNs

SMNs are rationally engineered with tailored structural parameters, including needle height, tip radius, base diameter, and array density.[23–25] This appropriate design can ensure efficient skin penetration (by avoiding nerve endings for minimal pain) while retaining robust mechanical integrity. Such performance is achieved *via* the selection of suitable materials, including stainless steel, titanium, silicon, and biocompatible polymers (*e.g.*, polycarbonate).[26–29] To attain efficient ISF extraction, the surface wettability of MNs can be flexibly regulated through multiple practical strategies.

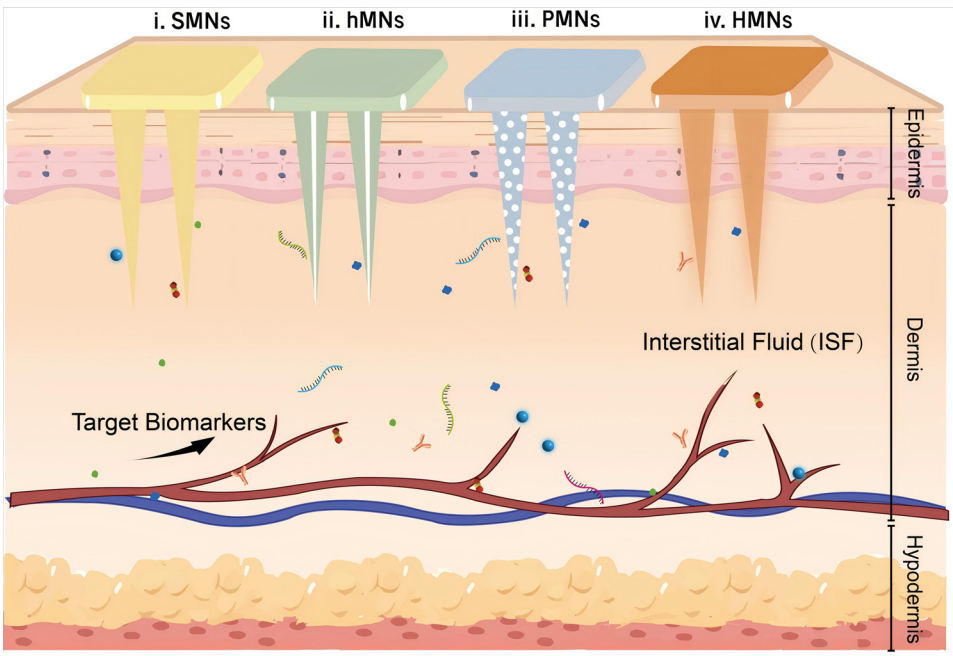

Fig. 1 Schematic representation of transdermal sampling using different types of tailorable MNs for ISF analysis, including (i) SMNs, (ii) hMNs, (iii) PMNs, and (iv) HMNs.

Hydrophilic functional groups are typically introduced *via* chemical modification or plasma treatment. Constructing micro/nano-scale rough structures or bionic architectures represents another effective method for enhancing the wettability of MNs. Additionally, MNs can be treated with hydrophilic coatings (*e.g.*, surfactant,[30] silicon oxide layer[31]), facilitating the adsorption capacity for ISF. A pivotal advantage of SMNs in MN-based biosensors are their capacity to enable painless, minimally invasive and repeated sampling of ISF or other biofluids/tissues, without inducing significant trauma, secondary infection, or requiring highly trained personnel, thus overcoming the inherent drawbacks of surgical excision and venipuncture. Specifically, within MN-based biosensor configurations, SMNs can fulfill two core functions: (i) serving as sampling tools to directly extract dermis-derived ISF, a well-recognized surrogate for blood that contains a wealth of biomarkers (*e.g.*, glucose, cytokines, and pathogens);[32–34] (ii) acting as transduction platforms when integrated with conductive materials (*e.g.*, gold nanoparticles, carbon nanotubes) or bio-recognition elements (*e.g.*, antibodies, aptamers) to achieve real-time, on-site monitoring of target analytes.[35,36]

2.2. Design of hMNs

hMNs are also rationally engineered with structural parameters including lumen diameter, length, tip geometry and wall thickness tailored for optimal performance.[37,38] hMNs are fabricated *via* advanced microfabrication techniques, such as laser drilling, photolithography, replica molding, 3D printing,[39–42] *etc*. Additionally, hydrophilicity of hMNs can be enhanced through laser exposure induced surface oxidation and photodegradation of the polymer backbone.[43] Biocompatible materials (*e.g.*, titanium and poly(lactic-*co*-glycolic acid)) are predominantly used for the fabrication of hMNs. In the design of MN-based biosensors, hMNs offer distinct advantages, whose intrinsic lumen enables direct and quantitative sampling of ISF with no sample dilution or loss,[44] which is superior to SMNs and invasive sampling methods (*e.g.*, venipuncture). Functionally, hMNs serve as precision sampling conduits for delivering biomarker molecules in ISF. Furthermore, hMNs also act as versatile, modifiable lumen interfaces for sensor element functionalization, enabling direct capture, recognition, and on-site analysis of target molecules in ISF. Collectively, hMNs enable integrated, sample-to-result diagnostic workflows with high translational potential.

2.3. Design of PMNs

PMNs are usually designed with numerous capillary channels and fabricated with polymers, metals, and inorganic materials. Their structural parameters include controlled pore size, high porosity, interconnected pores, and optimized height, tip radius, and array density.[45–47] PMNs are prepared *via* template replication, phase separation, electrospinning, or 3D printing.[48,49] A key advantage of PMNs lies in their microporous structure, which endows them with a larger specific surface area, thereby providing more active sites for target detection. For ISF extraction, PMNs can directly utilize their capillary-driven micro-channels for collecting fluid in the dermal layer. In addition, PMNs can be integrated with iontophoresis methods to enhance the delivery of ISF from the dermis to the sensing chamber for subsequent analysis.[50]

2.4. Design of HMNs

HMNs are generally designed to achieve efficient ISF extraction and integrated biosensing through their unique swelling properties.[51] HMNs are typically fabricated *via* mold casting of hydrophilic polymers (*e.g.*, hyaluronic acid, polyvinyl alcohol) that undergo physical or chemical crosslinking for solidification. This manufacturing approach offers the advantages of process simplicity, low cost, and scalability.[52–55] The key superiority of HMNs for sensing applications lies in their dual functionalities: (i) as an excellent immobilization matrix for biological recognition elements (*e.g.*, enzymes, antibodies, aptamers);[56,57] (ii) as an efficient medium for *in situ* ISF extraction and analyte enrichment. On the thermodynamic level, the driving force for ISF extraction mainly stems from the osmotic pressure difference between ISF and hydrogel networks of HMNs. After MNs are inserted into the skin, the introduction of counter ions or osmolytes into hydrogel networks will increase the Donnan osmotic pressure,[53,58,59] causing an expansion of the HMNs. The ISF extraction efficiency of HMNs is also governed by swelling kinetics.[60] When a HMN contacts with the dermis, ISF permeates its polymer matrix *via* intrinsic voids derived from local segmental motion, with subsequent relaxation of the polymer chains.[61] Hydrogels in HMNs can be allowed to swell under the polymer network's propagation and relaxation.[62] Generally, the nature of the polymer, degree of cross-linking, 3D structure, and porosity of hydrogels confer favorable thermodynamics and kinetics for ISF sampling *via* HMNs.[63–65] This integrated design enables simultaneous sampling, enrichment, and detection when combined with electrochemical transducers, significantly enhancing detection efficiency.[66–68] Practical implementations have demonstrated successful monitoring of biomarkers using HMNs, including glucose and ketones in ISF,[51,55] highlighting their great potential for point-of-care testing applications.

3. Construction of MN-based electrochemical biosensors

MN-based electrochemical biosensors are composed of microneedle units and electrochemical biosensing units, achieving biomarker monitoring in ISF. The construction of MN-based electrochemical biosensors for ISF biomarker analysis mainly follows two core integration modes: (1) a MN direct detection system based on a fully integrated three-electrode sensing configuration for achieving *in situ* electrochemical signal transduction upon skin insertion; (2) a MN-mediated detection system coupling ISF sampling and electrochemical detection of biomarkers. These two design paradigms, tailored for different application scenarios and detection requirements, have jointly

promoted the advancement of MN-based electrochemical biosensors in real-time and continuous ISF monitoring.

3.1. MN direct detection system

The MN direct detection system adheres to the classic electrochemical biosensing framework, consisting of a working electrode (WE), a counter electrode (CE), and a reference electrode (RE). The integration strategy varies according to the MN type, and the synergistic core lies in the coupling of the structural design of the MN module and the signal transduction of the electrochemical sensing module. For example, SMN-based electrochemical biosensors offer the most direct integration strategy. To design the WE, conductive modifications of SMNs can be achieved through either surface functionalization with conductive materials (*e.g.*, carbon nanotubes, graphene oxide and polyaniline) or internal coating with conductive composites,[68] followed by the immobilization of biorecognition elements (*e.g.*, antibodies, enzymes, and nucleic acids) to specifically capture target analytes.[69–72] By integrating a CE composed of chemically stable inert metals (*e.g.*, Pt, Au) with a RE (typically Ag/AgCl), the all-solid-state MN-based three-electrode system not only maintains structural mechanical stability to withstand skin insertion forces but also forms a reliable electrochemical interface, enabling direct *in situ* capture of biochemical analytes in ISF and their conversion into measurable electrochemical signals (*e.g.*, current, potential) upon transdermal penetration.[73–75] For PMNs and HMNs, the WE in the integration mode is further extended by pre-encapsulating conductive materials and biorecognition elements within the porous structure of PMNs or the hydrogel matrix of HMNs. The universal three-electrode configuration holds substantial potential for expanding the application scope of MN-based electrochemical biosensors, with particular relevance to chronic disease management, sports medicine, fitness monitoring, *etc*.

3.2. MN-mediated detection system

The MN-mediated detection system coupling ISF sampling units and electrochemical biosensing units is designed to sample sufficient ISF for biomarker monitoring. Different types of MN units in the design of MN-based electrochemical biosensors can be integrated with the electrochemical biosensing unit. For instance, hMNs and PMNs in MN-based electrochemical biosensors usually serve as the sampling units to extract ISF with the assistance of a micro-pump and through the inherent capillary from the phase-separated porous structure, respectively.[76–79] Subsequently, the collected ISF diffuses onto the pre-functionalized electrochemical interfaces of biosensing units (*e.g.*, screen-printed electrodes, microfluidic chips) to enable sensitive biomarker monitoring.[80,81] In contrast, HMNs offer a more streamlined sampling strategy, since they eliminate the need for a complex cavity or porous structural design. Upon transdermal insertion, HMNs can extract ISF efficiently based on thermodynamics and swelling kinetics,[59,82] allowing its direct transfer to coupled electrochemical sensing units.[83] This facilitates rapid, accurate and efficient biomarker quantification in subsequent steps.[84] The construction of MN-based electrochemical biosensors based on the MN-mediated detection system enables efficient collection and synergistic biomarker quantification of ISF through integrating diverse MN units with electrochemical biosensing units, thereby supporting POCT and clinical monitoring applications.

4. Monitoring biomarkers through MN-based electrochemical biosensors

Currently, MN-based electrochemical biosensors are widely applied for analysis of multiple biomarkers in ISF. Compared with single-point sensing, continuous longitudinal monitoring through these electrochemical biosensors can not only reveal fluctuation trends of biomarkers, but also find out the influences of individual variation, circadian rhythm and time evolution of pathophysiological processes on them.[85,86] For example, continuous glucose monitoring in personalized management of diabetes can dynamically reflect glucose fluctuations.[87] For drug therapy, the biosensors can cooperatively monitor the blood drug concentration and related biomarkers,[88,89] providing a basis for accurate drug use and efficacy evaluation.

As shown in Table 1, electrochemical biosensors based on different types of MNs have been successfully employed to monitor a wide range of biomarkers including metabolites, hormones, electrolytes, nucleic acids and proteins, achieving excellent analytical performance.

4.1. Monitoring of metabolic molecules

The real-time and continuous monitoring of metabolic molecules such as glucose, lactate, and uric acid is crucial for gaining a deep understanding of the body's metabolic activity and achieving precise diagnosis and treatment of metabolic diseases.[111–117] However, traditional detection methods (such as intermittent blood draws) have limitations, including high invasiveness and low temporal resolution, which restrict their application. Existing commercial devices with the ability of continuous monitoring mainly rely on enzymatic reactions, making them susceptible to environmental interference and unfavourable for the stable analysis of metabolic molecules. Therefore, it is necessary to develop new methods for the minimally invasive, efficient, and stable monitoring of metabolic analytes.

MN-based electrochemical biosensors have efficiently addressed these issues in a minimally invasive, continuous, and stable monitoring manner. For example, Poudineh *et al.*[90] developed an enzyme-free CGM device based on a low-cost HMN fabricated with a swellable dopamine (DA)–hyaluronic acid (HA) hydrogel (Fig. 2A). Modified with the synthesized silver–platinum nanoparticles (Ag–Pt NPs) and conductive poly (3,4-ethylenedioxythiophene) polystyrene sulfonate (PEDOT:PSS), the swellable conductive HMN array serves as the WE of the sensor. Meanwhile, an Au-coated MN acts as the CE and

Table 1 Comparison of the monitoring of diverse biomarkers *via* electrochemical biosensors based on different types of MNs

Target biomarkers	MN type	Electrochemical method	Sensing performance (sensitivity and LOD)	Ref.
Glucose	HMNs	Chronoamperometry	LOD 0.9 mM	90
	PMNs	Chronoamperometry	Sensitivity 22.99 ± 0.72 μA mM^{-1}	50
	hMNs	Chronoamperometry	Sensitivity 6.53 nA cm^{-2} mM^{-1}	78
Alcohol	SMNs	Chronoamperometry	Sensitivity 0.081 μA mM^{-1}	91
	hMNs	Chronoamperometry	Sensitivity 0.0452 nA mM^{-1}	92
Lactic acid	HMNs	SWV	LOD 1.04 mM	93
	HMNs	Amperometry	Sensitivity 0.003 ± 0.0004 μA mM^{-1}	94
	SMNs	Chronoamperometry	—	95
Cortisol	SMNs	DPV	LOD 0.22 nM	96
Insulin	SMNs	Amperometry	—	97
Progesterone	SMNs	DPV	LOD 100 aM	98
β-Estradiol			LOD 20 aM	
Ions (K^+)	SMNs	Potentiometry	Sensitivity 52.6–57.9 mV per decade, LOD $10^{-4.9}$ potassium activity	99
Ions (Na^+, K^+, Ca^{2+})	SMNs	Potentiometry	Sensitivity Na^+ 76.24 mV per decade, K^+ 47.1 mV per decade, Ca^{2+} 21.65 mV per decade	100
pH	SMNs	Potentiometry	Sensitivity 62.9 mV per pH	101
	HMNs	Chronoamperometry	—	102
	SMNs	Chronoamperometry	Sensitivity −57.2 mV per pH	25
cfDNA	HMNs	DPV	LOD 1.1 copies per μL	103
	SMNs	CV	LOD 1.1 fM	104
	SMNs	*i–t*	LOD 0.3 fM	105
CRP	HMNs	SWV	LOD 1.00 ng mL^{-1}	106
IL-6	SMNs	DPV/*i–t*	LOD 0.54 pg mL^{-1}	107
Tyr	SMNs	SWV	Sensitivity 5.52 ± 0.58 mA g^{-1} mL cm^{-2}, LOD 0.06 mg mL^{-1}	108
	hMNs	Amperometry	—	109
ErbB2	SMNs	DPV	Sensitivity 0.3978 μA cm^{-2} ng^{-1} mL, LOD 4.8 ng mL^{-1}	110

an Ag/AgCl MN acts as the RE, respectively. They utilized the HMN-based electrochemical biosensor for continuous monitoring from hyperglycemic to hypoglycemic ranges in a type 1 diabetic rat model. Similarly, Kumatani's and Takai's groups constructed PMN-based[50] and hMN-based[78] electrochemical biosensors for the monitoring of glucose, respectively.

To achieve multi-complexed monitoring of metabolites during daily activities, Xu *et al.*[91] reported a fully integrated microneedle biosensor that simultaneously measures fitness-related biomarkers (*e.g.*, glucose, lactate, and alcohol) during physical exercise (Fig. 2B). Such a wearable sensor integrates a biocompatible 3D-printed SMN array that can comfortably access skin interstitial fluid and a small circuit for signal processing and calibration, and wireless communication. Based on a series of enzymatic reactions, they developed SMN-based electrochemical biosensors that could monitor fitness-related biomarkers across multiple subjects and support multi-day monitoring, with results showing a good correlation with commercial devices. The biosensing strategy has the potential to boost intelligent wearable devices in sports health.

Despite the aforementioned advancements achieved by existing SMN-based electrochemical biosensors, they still suffer from inherent drawbacks: (1) SMNs are usually surface-functionalized with enzymes, antibodies, or aptamers that tend to detach during skin insertion, leading to marked declines in measurement accuracy and device lifespan.[85,118] (2) Their incompatible rigid nature with the soft, flexible skin causes physical displacement during *in vivo* measurements, resulting in severe measurement instability.[86] The limitations underscore the urgent need for a new type of skin-compatible, mechanically robust, and analytically stable MN-based biosensing technology to enable reliable and continuous *in vivo* monitoring. Poudineh's group developed a Wearable Aptalyzer that integrates methacrylated hyaluronic acid (MeHA) HMN arrays with an electrochemical aptasensing module for real-time, continuous, dual monitoring of glucose and lactate (Fig. 2C).[93] Upon skin insertion, the HMN patch swells to facilitate the diffusion of target analytes toward aptamer-functionalized electrodes, with aptamers not directly exposed to ISF for avoiding probe damage *in vivo*. Instead, HMN patches are hybrid-integrated with three-electrode electrochemical chips, which address the inherent limitations of SMNs by providing a biocompatible, flexible yet mechanically robust platform for ISF extraction and stable sensing. Furthermore, the binding-induced conformational change of the aptamer alters the electron transfer efficiency between methylene blue and the electrode surface, and the resulting electrochemical signal could be detected *via* square wave voltammetry (SWV). Compared with enzymatic detection methods, the design combining aptamers into HMN-based electrochemical biosensors enables continuous, reliable, and multiplexed biomonitoring *in vivo*.

4.2. Monitoring of hormones

The dynamic changes in hormone levels can directly reflect the functional status of target organs, providing crucial information with long timelines and tissue specificity for assessing physiological states and diagnosing endocrine-related diseases.[87–89,119] Recently, ISF-based testing enables the continuous capture of the dynamic fluctuation patterns of hor-

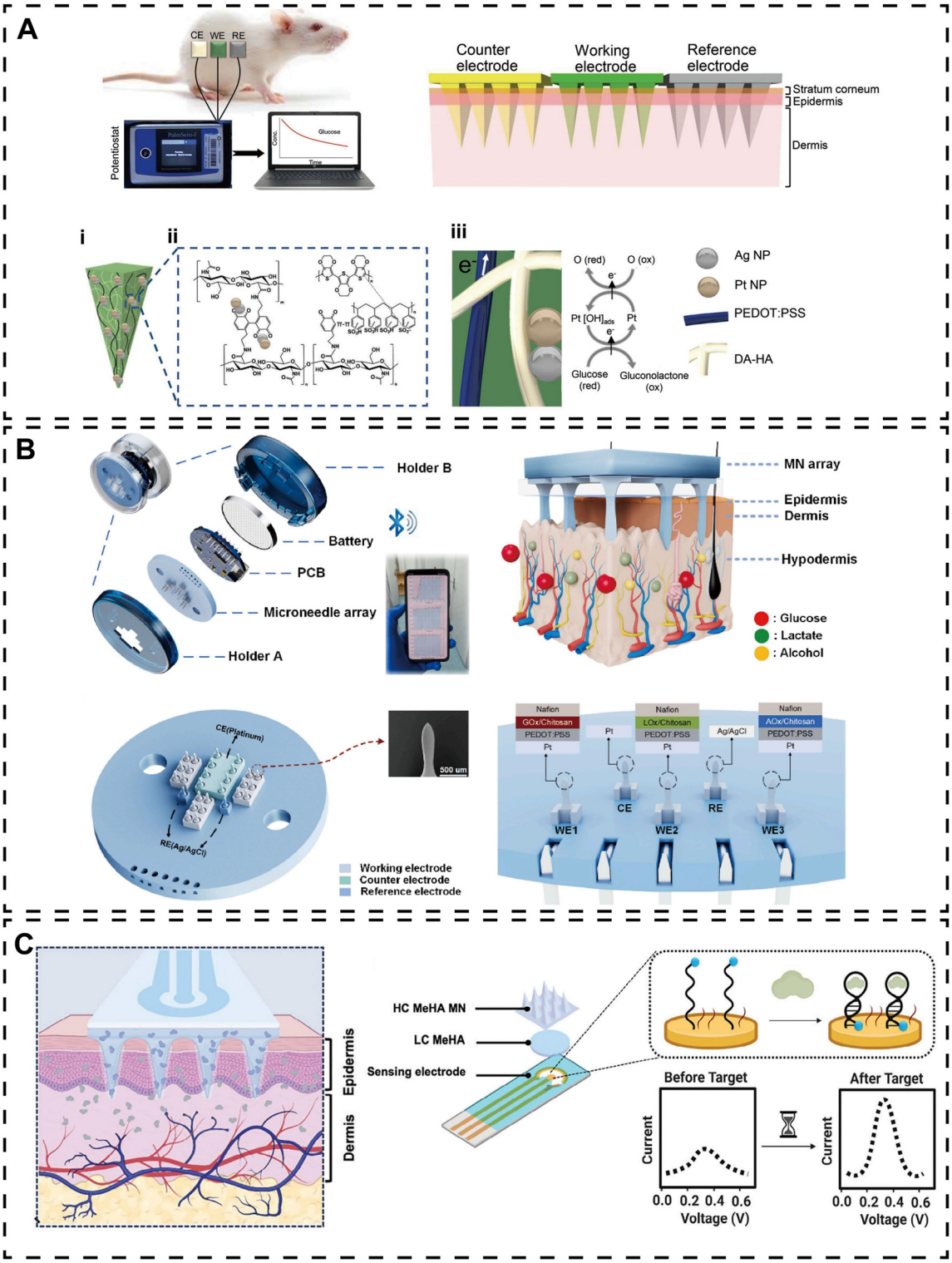

Fig. 2 MN-based electrochemical biosensors for monitoring metabolic molecules. (A) Schematic diagram of a conductive hydrogel MN-based electrochemical biosensor for continuous glucose monitoring.[90] Reproduced with permission from ref. 90. Copyright 2022, John Wiley & Sons, Inc. (B) Schematic design of an MN-based enzymatic electrochemical biosensor for alcohol monitoring.[91] Reproduced with permission from ref. 91. Copyright 2024, Elsevier. (C) Schematic diagram of a hydrogel microneedle-based electrochemical aptasensor for the synchronous monitoring of lactate and glucose.[93] Reproduced with permission from ref. 93. Copyright 2024, John Wiley & Sons, Inc.

mones, providing real-time physiological insights for early disease warning and the formulation of personalized treatment strategies that are difficult to obtain with traditional blood testing methods.

To achieve the effective monitoring of cortisol, Guo *et al.*[96] designed a conductive SMN-based aptasensor by using polylactic acid as the microneedle substrate and constructing a conductive interface through gold plating and electrodeposition of dendritic gold nanoparticles (Fig. 3A). Based on the conformational changes of the aptamer after binding to the target molecule, sensitive detection of cortisol was achieved with a "signal on" response *via* differential pulse voltammetry (DPV). The conductive SMN-based electrochemical aptasensor exhibited a wide detection range (1–1000 nM), a detection limit of 0.22 nM in simulated ISF. Another example stems from the study of Voelcker's group.[97] They developed a transdermal electrochemical sensing platform by integrating a 3D-printed polymer lattice (PL) protective membrane onto the surface of a gold-plated microneedle (PL-pMNA), for quantitative analysis of insulin by immobilizing specific aptamers (Fig. 3B). It achieved linear detection within the range of 0.2–2 nM and demonstrated excellent skin penetration capability and signal stability in pig skin experiments. Their strategy based on micro-processing protective microstructures opens new pathways for developing next-generation high-performance, durable wearable transdermal electrochemical sensing devices.

Furthermore, MN-based electrochemical biosensors have also been extended to the field of sex hormone monitoring.

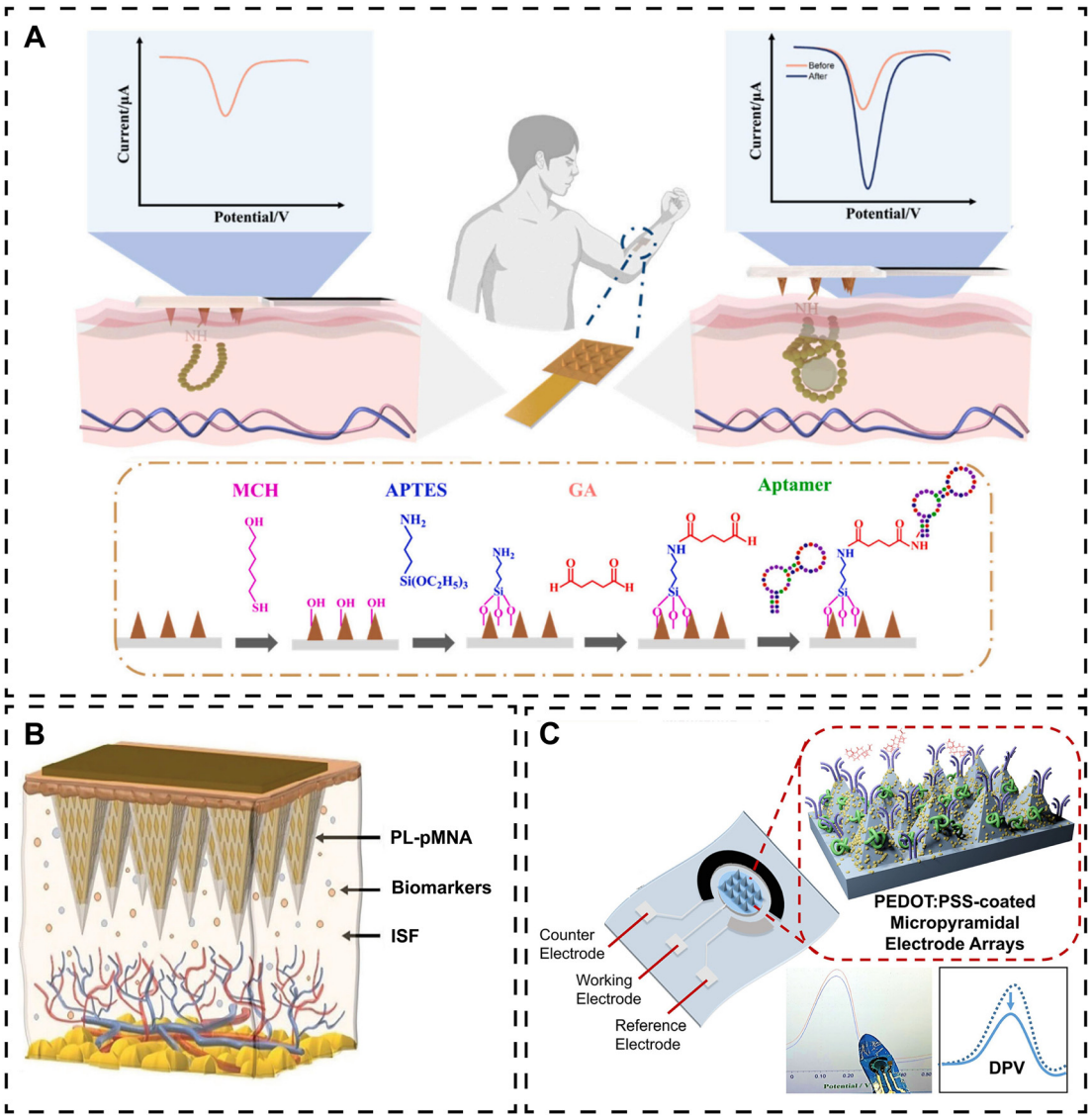

Fig. 3 MN-based electrochemical biosensors for the monitoring of hormones. (A) Schematic description of a conductive MN-based electrochemical aptasensor for cortisol monitoring.[96] Reproduced with permission from ref. 96. Copyright 2024, Elsevier. (B) Scheme of a 3D-printed polymer lattice-protected Au-microneedle for aptamer-based insulin monitoring.[97] Reproduced with permission from ref. 97. Copyright 2024, John Wiley & Sons, Inc. (C) Schematic description of microneedle electrodes based on flexible conductive polymers for monitoring of sex hormones.[98] Reproduced with permission from ref. 98. Copyright 2023, American Chemical Society.

Progesterone (P4) and β-estradiol (E2), as two key sex hormones, show level fluctuations closely related to female reproductive health and fertility.[120–122] As shown in Fig. 3C, Xie *et al.*[98] reported a flexible electrochemical immunosensor based on a PEDOT:PSS-coated three-dimensional MN array. As shown in Fig. 3C, the specific P4 and E2-antibodies were immobilized on the MN surface of the electrochemical immunosensor *via* electrochemically deposited gold nanoparticles for capturing P4 and E2. The MN-based electrochemical immunosensor presented ultra-high sensitivity detection of P4 and E2 with detection limits reaching 100 aM and 20 aM, respectively, and a wide linear range spanning six orders of magnitude (1 fM–1 μM and 10 aM–1 μM) *via* DPV. This biosensor has been successfully applied for the long-term dynamic monitoring of hormone levels throughout the female menstrual cycle, providing a powerful tool for home-based, convenient health management.

4.3. Monitoring of electrolytes

Electrolyte balance is essential for maintaining the body's physiological homeostasis, since its dynamic changes directly reflect the real-time status of nerve conduction, muscle movement, and metabolic activity. For example, sodium (Na^+) is a prominent prognostic biomarker for assessing disorders such as hyponatremia and hypernatremia, which strongly predict risks in hospitalized and ICU patients with heart failure,[123] coronavirus (COVID-19) infection,[124] and chronic kidney disease.[125] Abnormal potassium (K^+) fluctuations are recognized as early indicators of alcoholism, heart disease, AIDS, diabetes, and cancer.[126] Based on epidermis electrophysiological recording and sweat detection, Rogers's group developed conformal coatings as ultra-soft elastomeric substrates with advanced fluid management, excellent biomechanical compatibility, environmental adaptability (*e.g.*, waterproofing, contamination resistance) for multimodal sensing,[127,128] *etc*. In contrast, MNs enable direct access to ISF *via* transdermal penetration, featuring minimally invasive sampling, rapid analysis, as well as targeted delivery potential. For example, Crespo and his colleagues proposed a wearable all-solid-state microneedle patch for intradermal potentiometric monitoring of K^+ in ISF (Fig. 4A).[99] The SMNs were modified with functionalized multiwalled carbon nanotubes (f-MWCNTs) and Ag/AgCl coatings to fabricate the K^+-selective working electrode and the reference electrode, respectively. The SMN-based electrochemical biosensing patch exhibited a detection limit of $10^{-4.9}$ potassium activity, a linear range of $10^{-4.2}$ to $10^{-1.1}$, and a drift of 0.35 ± 0.28 mV h^{-1}. Measurement experiments of *ex vivo* intradermal K^+ in chicken and porcine skin confirmed the microneedle patch's suitability for monitoring skin K^+ changes. Coupling these two technologies yields a synergistic hybrid system, which will overcome the limitations of individual technologies in special extreme environments (*e.g.*, tissue fluid exudation and skin dryness settings) of clinical scenarios. It is expected to achieve multifunctional integration from high-fidelity electrolyte detection, further enhancing the system's practicality and applicability.

Compared with single biomarker detection, monitoring different types of ions (*e.g.*, Na^+, K^+, Ca^{2+}) simultaneously could provide more comprehensive information feedback for more accurate diagnosis of diseases related to physiological ion changes. However, this brings more stringent requirements and heightened challenges for manufacturing different types of sensors with 3D microneedle arrays and adjusting the functionalization of their closely spaced tips, which is more complex than processing planar electrodes. To overcome these limitations, Xie *et al.*[100] developed a multiplexed biosensing array assembling planar microneedle chips manufactured by laser micromachining, achieving real-time, simultaneous monitoring of Ca^{2+}, K^+, and Na^+ in ISF. As shown in Fig. 4B, the MN-based electrochemical biosensing array integrates three modules, including an ion-sensing MN array (ISMA) electrochemically deposited with a gold layer and a PEDOT:PSS conductive polymer layer, a recording/control printed circuit board, and a real-time monitoring mobile application. The ISMA *in vivo* exhibited potentiometric responses at physiologically relevant concentrations of 0.01–100 mM for Ca^{2+}, 1–32 mM for K^+, and 10–160 mM for Na^+, indicating its excellent multi-ion-sensing ability in subcutaneous tissue fluids.

As another important biomarker, the concentration of H^+ or the pH level can reveal changes in electrolyte concentration or ion distribution, reflecting the acid–base balance status and microenvironment homeostasis.[101,129–131] It has been reported that the pH level serves as a vital indicator of numerous pathophysiological states, including ischemia, multiple sclerosis, insulin resistance, peripheral artery disease, stress, tumor size, acute respiratory distress, *etc*.[132–136] Unlike the well-buffered blood, ISF pH can vary considerably under metabolic stress, such as in tumors or chronic wounds where it can drop below 6.0. This variability makes ISF pH a valuable diagnostic marker.[137] Consequently, the development of wearable sensors for continuous and minimally invasive monitoring represents a promising pursuit. For example, Voelcker *et al.*[101] proposed a wearable biosensor based on a high-density polymer microneedle array (PMNA) for real-time transcutaneous potentiometric monitoring of pH in ISF. As shown in Fig. 4C, the PMNA was prepared by injecting the OrmoComp® photocurable polymer and performing UV curing *via* soft lithography. This PMNA-based wearable biosensor employed a polyaniline (PA)-coated PMNA as the WE, and the microneedle substrate was modified with an insulating layer to exclude interference from other body fluids such as sweat. The PMNA-based electrochemical biosensor exhibited high sensitivity of 62.9 mV per pH unit and high accuracy of ±0.036 pH units within the pH range of 4.0–8.6, and possessed excellent anti-interference ability, reproducibility, and long-term stability. Wearing testing experiments on mouse skin further verified that this biosensor can monitor transcutaneous ISF pH changes in real-time and accurately.

4.4. Monitoring of nucleic acids

Nucleic acids, as key molecular biomarkers present in blood and interstitial fluid, hold significant value in early cancer screening, diagnosis of infectious diseases, monitoring of

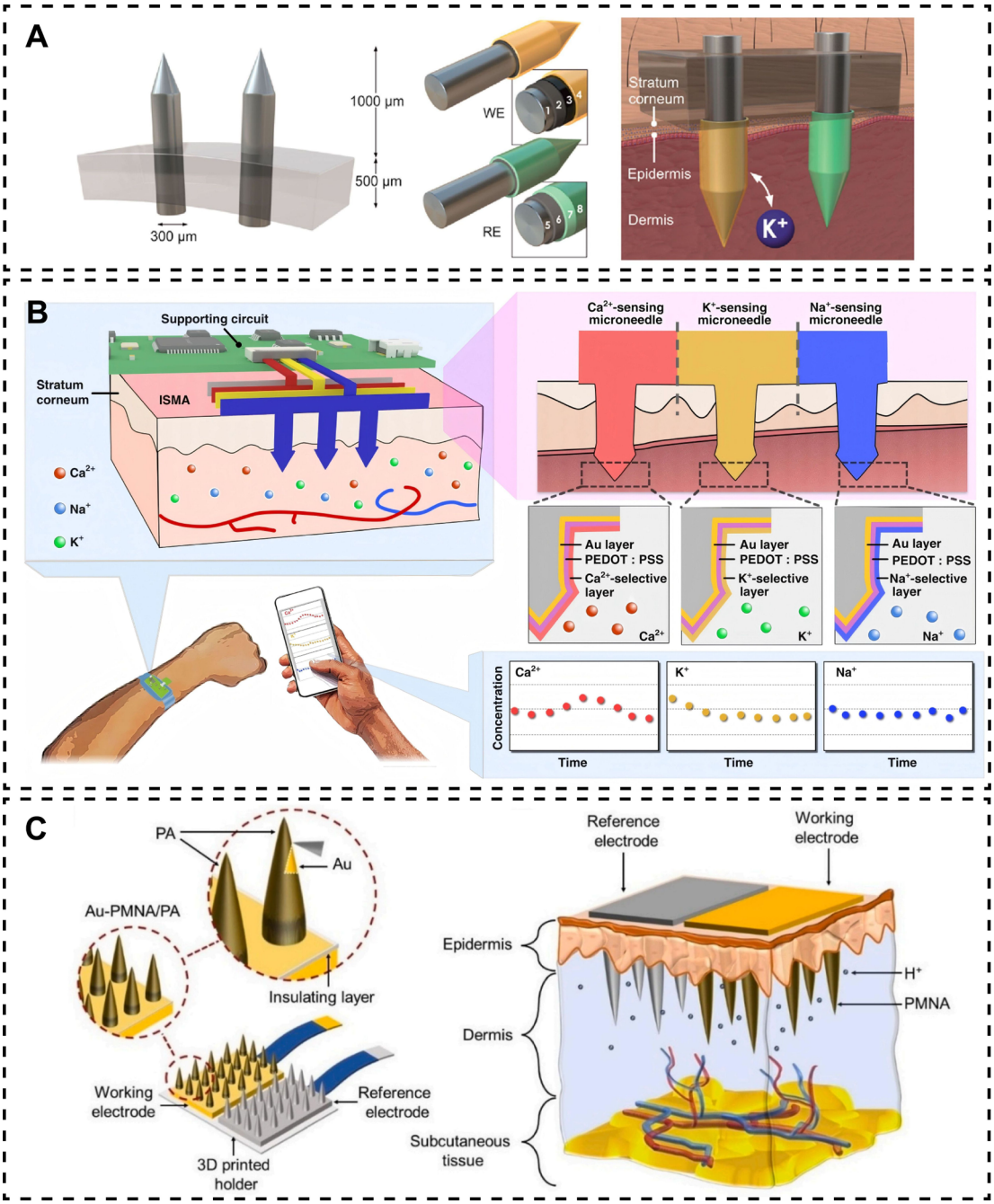

Fig. 4 MN-based electrochemical biosensors for monitoring electrolytes. (A) Schematic diagram of the wearable all-solid-state potential microneedle patch for intradermal potassium monitoring.[99] Reproduced with permission from ref. 99. Copyright 2018, American Chemical Society. (B) Schematic diagram of a 3D-assembled laser-microfabricated MN-based ion-sensing array for multiplexed monitoring of Ca^{2+}, K^+, and Na^+ in ISF.[100] Reproduced with permission from ref. 100. Copyright 2023, Springer Nature. (C) Schematic diagram of a polyaniline-modified functionalized MN array for *in vivo* pH sensing.[101] Reproduced with permission from ref. 101. Copyright 2022, Elsevier.

transplant rejection, and management of critically ill patients.[138,139] Compared with traditional tissue biopsy, the structural basis of wearable MN-based sensors for *in vivo* nucleic acid detection possesses the unique advantages of being minimally invasive and dynamically reflecting the disease status. Recently, MN-based electrochemical biosensors combined with functional nucleic acid recognition elements [*e.g.*, framework nucleic acid and clustered regularly interspaced short palindromic repeats (CRISPR)] and highly sensitive electrochemical transduction interfaces have achieved the integration of extraction, recognition, and signal output for ultratrace nucleic acids.

Taking cell-free DNA (cfDNA) as an example, the detection of Epstein–Barr virus cell-free DNA (EBV cfDNA) in ISF poses a

huge challenge in molecular diagnostics. While conventional techniques such as the polymerase chain reaction (PCR) and genotyping can identify its presence, they often fall short in enabling rapid, specific isolation of target nucleic acids and long-term real-time monitoring, thereby limiting dynamic disease surveillance. To address this limitation, Yang *et al.*[140] developed a HMN-based biosensing patch (Fig. 5A) for the rapid *in situ* capture of EBV cfDNA from ISF within approximately 15 minutes, achieving a maximum capture efficiency of 93.6%. Crucially, this system integrated a wearable flexible microfluidic device with electrochemical recombinase polymerase amplification (eRPA), enabling the quantitative analysis of the captured EBV cfDNA with a detection limit of 3.7×10^2 copies per μL. *In vivo* experiments convincingly validated the patch's capture and analytical performance for EBV cfDNA. To further expand the capabilities for cfDNA extraction and real-time monitoring, Yang *et al.*[104] subsequently constructed a wearable MN patch leveraging the synergistic effect of a graphene bio-interface and the CRISPR-Cas9 system (Fig. 5B). For real-time cfDNA monitoring, they integrated a spray-on functional flexible PDMS patch and a three-electrode conductive MN array into a wearable platform. The process involved depositing carbon nanotubes (CNTs) onto a hydrophilic-modified PDMS membrane, where the patterned CNTs functioned as a reverse iontophoresis (RI) chamber to separate negatively charged molecules such as nucleic acids. A conductive CRISPR-functionalized MN array, serving as the working electrode, was then connected to the anode side of the CNT pattern. During real-time detection, the MNs penetrate the epidermis to isolate and enrich the target DNA, which is specifically recognized by the Cas9/sgRNA complex immobilized on the MN surface. The resulting CRISPR-mediated cleavage event is transduced into a quantifiable signal change *via* an integrated three-electrode system. This wearable MN platform demonstrated the capability for real-time monitoring of cfDNA from EBV, sepsis, and kidney transplant rejection.[103] Validation experiments in an immunodeficient mouse model confirmed the feasibility and practicality of this approach, highlighting its potential for *in vivo* monitoring of cfDNA for early disease screening and prognostic evaluation.

Pushing the boundaries of long-term stability even further, Yang and his colleagues also fabricated a wearable device based on Natronobacterium gregoryi Argonaute (NgAgo, an endonuclease) and tetrahedral DNA nanostructures (TDNs) for the continuous monitoring of ultra-trace nucleic acids *in vivo*.[105] This wearable system initiates the detection procedure by using a functional thermoplastic polyurethane (TPU) film to enrich nucleic acids from ISF *via* reverse iontophoresis (Fig. 5C). The collected analytes are then detected at the interface of a three-electrode MN patch. Specifically, the graphene surface on the MN patch is engineered with rigid tetrahedral DNA nanostructures (TDNs), which serve as precisely oriented nano-scaffolds to optimize the probe orientation and enhance the sensing signal. The NgAgo/guide DNA (NgAgo-gDNA) composite immobilized on these TDN-17 performs the molecular recognition by specifically binding to target nucleic acids through Watson–Crick base pairing. Finally, the binding event is transduced into an electrical signal, which is managed and

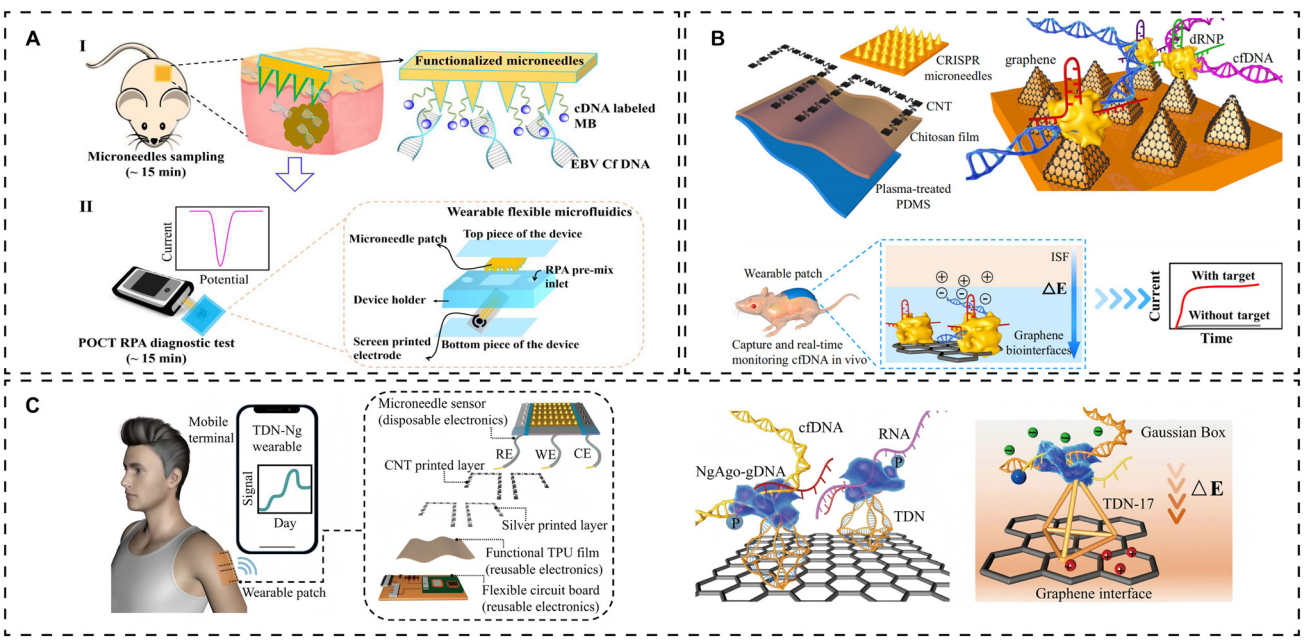

Fig. 5 MN-based electrochemical biosensors for *in vivo* nucleic acid monitoring. (A) Schematic illustration of an HMN-based biosensing platform for rapid capture and detection of EBV cfDNA.[140] Reproduced with permission from ref. 140. Copyright 2019, American Chemical Society. (B) Scheme of a CRISPR-Cas9-integrated microneedle patch for cfDNA detection.[104] Reproduced with permission from ref. 104. Copyright 2022, Springer Nature. (C) Scheme of a reverse iontophoresis-based microneedle patch for cfDNA capture and detection.[105] Reproduced with permission from ref. 105. Copyright 2024, Springer Nature.

wirelessly transmitted by the integrated flexible circuit board for real-time, continuous monitoring. Integrating with the engineered NgAgo biorecognition interface, the device could stably monitor intracellular cfDNA and RNA in real-time for up to 14 days, with a detection limit of 0.3 fM. This wearable device provides a valuable framework for real-time and long-term *in vivo* nucleic acid monitoring.

4.5. Monitoring of proteins

Proteins found in serum, tissue, or body fluids are critical biomarkers for disease diagnosis, therapeutic response evaluation, and health monitoring. Over 1500 clinically validated protein biomarkers (*e.g.*, human epidermal growth factor receptor 2, beta-amyloid, inflammatory cytokines, and cancer antigen 125) have been identified so far, enabling dynamic tracking of pathophysiological changes involved in oncology, cardiology, and immunology. Detecting these protein biomarkers in ISF is a promising alternative to blood-based detection, but it faces huge challenges. First, protein concentrations in ISF are far lower than in serum. Second, the dense extracellular matrix in ISF can hinder molecular interactions. Third, conventional ISF sampling and analysis methods lack real-time continuity. MN-based electrochemical sensors offer distinct advantages for addressing these challenges. They enable minimal invasiveness and *in situ* extraction integrated with biosensing of ISF. They also provide high sensitivity and real-time readout, as well as compatibility with continuous monitoring. Moreover, these biosensors will overcome the invasiveness, long processing times and discontinuous nature of traditional serological assays such as enzyme-linked immunosorbent assays (ELISA) and mass spectrometry.

Currently, C-reactive protein (CRP) has been identified as a key biomarker of inflammation and bacterial infections, with significant implications for their early diagnosis and disease monitoring.[141–144] For instance, Yuan *et al.*[106] integrated an ultra-swelling microneedle aptamer-recognition tester (uSMART) for detecting CRP toward point-of-care monitoring of bacterial infections and treatment. As shown in Fig. 6A, this MN-based aptasensing platform consists of two functionally complementary modules. Among them, the ultra-swelling MN sampling module based on methacrylated hyaluronic acid/sodium hyaluronate (HAMA/SH) enables minimally invasive and efficient extraction of ISF. The synergistic biosensing module containing a hierarchical flower-like gold nanostructure-decorated screen-printed carbon electrode (HFGN-SPCE) immobilized with aptamers can carry out reagentless, highly selective detection of CRP. Through a target-induced aptamer recognition mechanism, this uSMART system exhibits a wide linear range (1 ng mL^{-1} to 100 μg mL^{-1}), a detection limit as low as 0.85 ng mL^{-1}, excellent selectivity, repeatability, and long-term stability for CRP detection. Integrated with a microelectrochemical workstation containing a Bluetooth wireless transmission unit and a smartphone APP, the uSMART platform has been successfully applied *in vivo* for continuous monitoring of CRP throughout the entire process of methicillin-resistant *Staphylococcus aureus* infection and vancomycin treatment. In addition, monitoring dynamic changes of cytokines is an important window

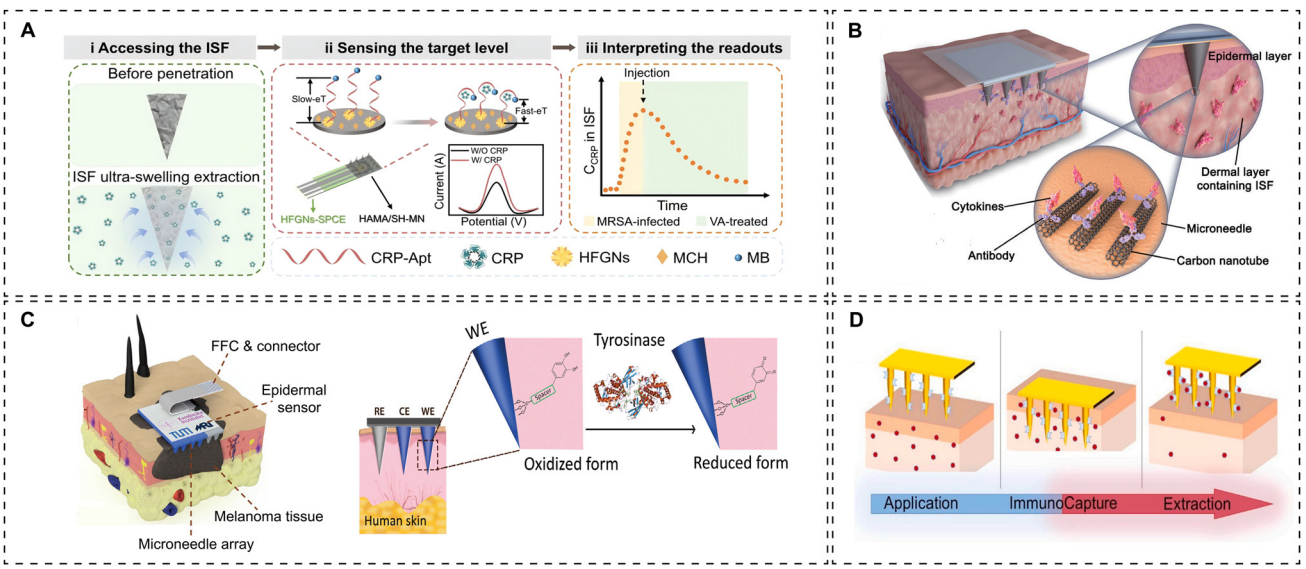

Fig. 6 MN-based electrochemical biosensors for protein monitoring. (A) Schematic illustration of an integrated superswelling microneedle aptasensing platform for C-reactive protein monitoring.[106] Reproduced with permission from ref. 106. Copyright 2025, American Chemical Society. (B) Schematic illustration of a carbon nanotube biointerface-based microneedle patch for cytokine monitoring.[107] Reproduced with permission from ref. 107. Copyright 2023, John Wiley & Sons, Inc. (C) Schematic illustration of a chemically responsive probe-modified epidermal microneedle biosensing patch for Tyr monitoring.[108] Reproduced with permission from ref. 108. Copyright 2024, John Wiley & Sons, Inc. (D) Schematic illustration of a gold-coated silicon microneedle electrochemical immunosensing patch for ErbB2 monitoring.[110] Reproduced with permission from ref. 110. Copyright 2021, Elsevier.

for assessing pathological states such as sepsis and autoimmune diseases. As shown in Fig. 6B, Fang's group developed a conductive SMN-based immunosensing patch by sputtering an Au layer and dropping a chitosan-aminated carbon nanotube (CNT) film on an SU-8 photoresist MN array.[107] This wearable MN immunosensor employed CNT-functionalized conductive microneedles for minimally invasive penetration of the epidermal layer to access the ISF in the dermal layer. Once the SMN-based immunosensing patch is deployed, interleukin-6 (IL-6) antibodies immobilized on the microneedle surface specifically capture target cytokine IL-6 in ISF. The specific binding of antigens to antibodies alters charge transfer and increases steric hindrance at the electrode interface. This biochemical interaction is effectively converted into a quantifiable electrical signal. The system monitors these current changes in real-time, enabling the *in situ* quantification of cytokine biomarkers directly within the body. Through *in situ* electrochemical analysis, ultra-high sensitivity detection was achieved (detection limit 0.54 pg mL^{-1}) by the SMN-based immunosensor, and provided successful early warning of rising IL-6 concentrations within 1–4 hours in a rat sepsis model. Similarly, Beker's, Wen's, and Kelley's groups have also presented a series of MN-based electrochemical biosensors for monitoring vascular endothelial growth factor (VEGF),[145] immunoglobulin G (IgG),[146] and tumor necrosis factor-α (TNF-α),[147] respectively.

In the field of monitoring tumor-related protein biomarkers, tyrosinase (Tyr) is one of the key biomarkers, and its activity level is closely related to the occurrence and progression of melanoma.[148–150] Hence, achieving rapid and sensitive detection of Tyr is of great significance for the early screening of melanoma, assessment of mole transformation risk. Parlak *et al.*[108] constructed an electrochemical biosensing patch based on PEDOT:PSS composite conductive microneedles (Fig. 6C) for monitoring Tyr. To fabricate the electrochemical biosensing patch, the composite microneedle arrays composed of polyurethane (PU) and PEDOT:PSS were integrated with a surface-bound chemo-responsive smart probe to enable target-specific electrochemical detection of Tyr directly from skin tissue. In the novel design, a Tyr-responsive biointerface was constructed through successive modification of silanization and cross-coupling of l-3,4-dihydroxyphenylalanine (L-dopa) as the probe. Tyr can catalyze the oxidation of L-dopa to dopaquinone, which is transduced into a representative SWV signal with the "signal on" principle detected by the integrated epidermal sensor device. This conductive MN-based electrochemical biosensor exhibited a linear range of 0.3–0.7 mg mL^{-1}, with a detection limit of 0.06 mg mL^{-1}, good specificity, stability, and reproducibility (RSD < 5%). The completed continuous monitoring for 3 days on an *ex vivo* healthy human skin tissue injected with different Tyr concentrations indicates its potential as an alternative for fast and reliable diagnosis of melanoma and the evaluation of skin moles.

Expanding their application beyond chemical probes, MN-based electrochemical biosensors have been adapted for immunoassays by conjugating with antibodies. This capability is crucial for detecting protein biomarkers like human epidermal growth factor receptor 2 (ErbB2), which is vital for the early detection, subtype classification, and therapy evaluation of breast cancer.[151,152] To this end, Voelcker *et al.*[110] developed an electrochemical immunosensor based on a high-density silicon MN array for ErbB2 detection. They utilized ultraviolet lithography and deep reactive ion etching technology to fabricate a gold-coated silicon MN array, which serves as both an extraction platform for biomarkers and an electrochemical signal transduction interface (Fig. 6D). By covalently immobilizing ErbB2-specific antibodies *via* a self-assembled monolayer, the biosensor achieved highly selective immune recognition and quantitative analysis of the target ErbB2. Based on this, the electrochemical immunosensor exhibited a low detection limit (4.8 ng mL^{-1}) for ErbB2 in artificial ISF, which is lower than the expected ErbB2 level in breast cancer patients (65.38 ng mL^{-1}), indicating its great potential for detecting ErbB2 in clinical samples. Besides growth factor biomarkers, vascular endothelial growth factor (VEGF),[145] phosphorylated tau proteins (P-tau 181 and P-tau 217),[153] monkeypox virus A29 protein,[154] both CRP and IL-6[155] have also been monitored using MN-based electrochemical immunosensors.

4.6. Monitoring of multiple types of biomarkers

Synchronous monitoring of multiple biomarkers is essential for the comprehensive management of disease and its complications, yet significant challenges persist in developing effective MN-based electrochemical biosensors. The complex composition of ISF demands sensing units that guarantee both high specificity and sensitivity for simultaneous detection. A fundamental limitation lies in the instability of enzyme or antibody-based sensing interfaces, whose performance inevitably degrades due to denaturation and susceptibility to biofouling *in vivo*. Furthermore, the integration of multi-discrete sensing units onto a single miniaturized microneedle platform without signal crosstalk presents a major engineering hurdle. Overcoming these obstacles is critical for realizing reliable, long-term monitoring that can reveal a patient's health status.

Inspired by the needle-like spikes's structure and function on the barbed tongue of felines, Xie's group developed a self-calibrating multiplexed MN electrode array (SC-MMNEA) capable of real-time, continuous, and synchronous POC monitoring of multiple biomarkers including glucose, cholesterol, uric acid, lactate, ROS, Na^+, K^+, Ca^{2+}, and pH in ISF.[156] As shown in Fig. 7A, comprising a multi-analyte MN array sensor, a self-calibration module, and an electronic circuit module, the SC-MMNEA system features single-analyte-specific detection per MN. This design effectively solved the crosstalk problem associated with direct chemical modification of the MN patch. The self-calibration module uses hMNs to deliver a known-concentration solution into ISF; meanwhile, adjacent MN electrochemical electrodes rapidly measure the target analyte's local ISF concentration. This MN-delivery-mediated self-calibration technique could address the inherent problem of decreased accuracy of implantable electrodes caused by long-term tissue variation and enzyme degradation, enhancing the

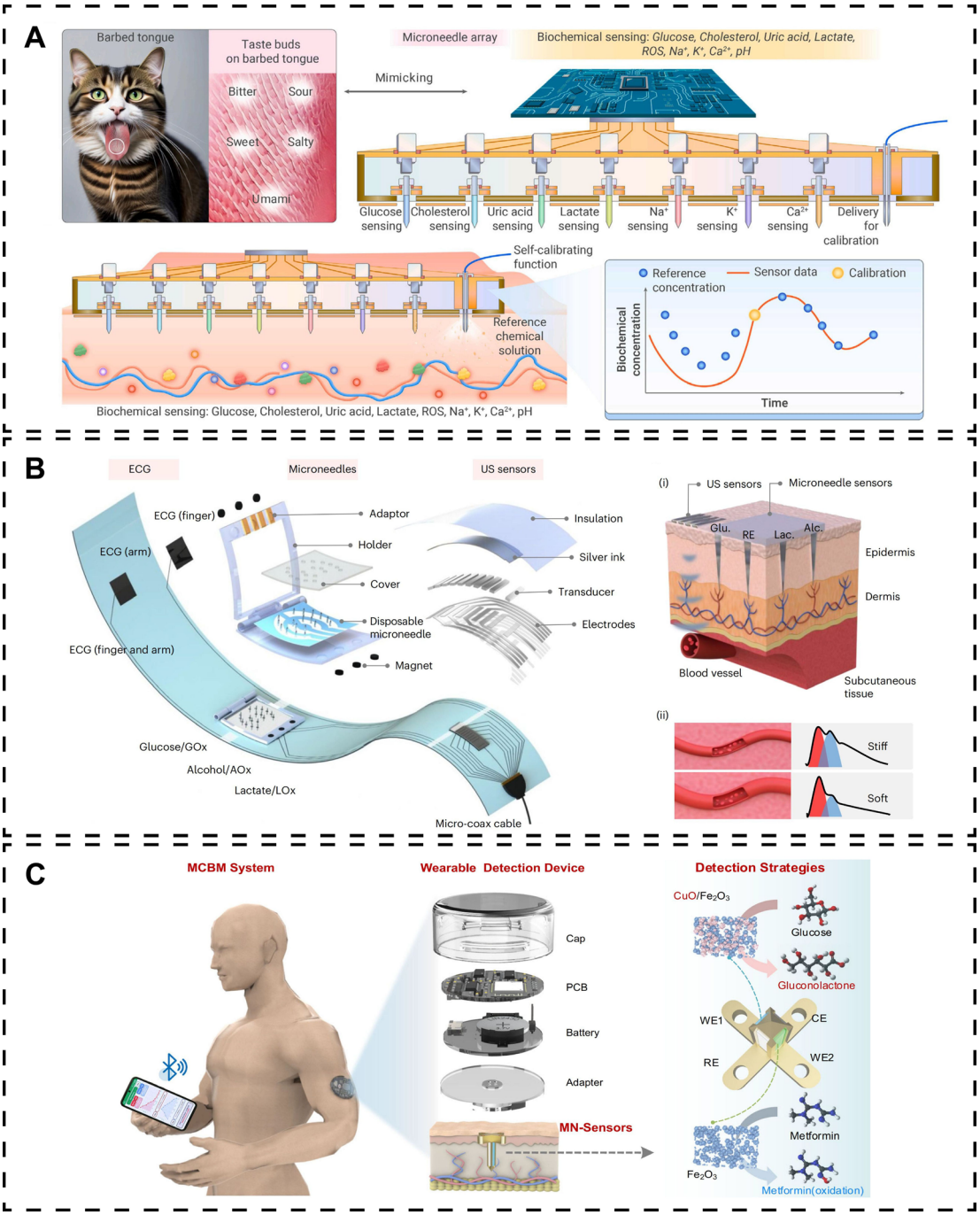

Fig. 7 MN-based electrochemical biosensors for multiple types of biomarkers. (A) Schematic diagram of a self-calibration multiplex microneedle array for subcutaneous multiple analyte monitoring.[156] Reproduced with permission from ref. 156. Copyright 2025, Elsevier. (B) Schematic diagram of an MN-based multiplex chemical–physical sensor for monitoring diabetic metabolites and cardiac signals.[157] Reproduced with permission from ref. 157. Copyright 2025, Springer Nature. (C) Schematic illustration of an MN-based integrated pharmacokinetics and pharmacodynamics evaluation platform for simultaneous monitoring of diabetes biomarkers and drugs.[158] Reproduced with permission from ref. 158. Copyright 2025, Springer Nature.

reliability of the MN sensors. *In vivo* experiments applied in both healthy and diabetic rat models indicated that SC-MMNEA could provide real-time POC monitoring of multiplexed analyte concentrations with good accuracy, especially after self-calibration. The proposed SC-MMNEA has the advantages of *in situ* and minimally invasive monitoring of health states and the potential to facilitate wearable diagnostic devices for long-term monitoring of multiple types of biomarkers *in vivo*. To advance the development of effective diabetes management, comprehensive glycemic control usually

relies on chemical and physical inputs (affecting disease pathophysiology and reflecting cardiovascular risks), rather than a single glucose signal. To achieve this goal, Wang and his colleagues created a hybrid flexible wristband integrating a microneedle array for sensing multiplexed biomarkers (*e.g.*, glucose, lactate, alcohol) and an ultrasonic array for monitoring blood pressure, arterial stiffness and heart rate (Fig. 7B).[157] This multimodal system enables continuous POC evaluation of the metabolic and cardiovascular status, supporting glycemic control and cardiovascular risk alerting. It captures the interplay between ISF biomarkers and physiological parameters during daily activities, expanding diabetes monitoring beyond tracking a single type of metabolic biomarker to address limitations of existing systems and enhance the management of diabetes and related cardiovascular risks.

To achieve precise and personalized disease management, the simultaneous monitoring of drugs and disease-related biomarkers is also crucial for tracking real-time pharmacodynamic effects, guiding precise medication adjustments and optimizing individualized treatment outcomes. Jiang and his collaborators proposed a microneedle-based continuous biomarker/drug monitoring (MCBM) system that features a dual-sensor MN with a layer-by-layer nanoenzyme immobilization strategy (Fig. 7C).[158] Leveraging 3D-printed MN channels and differential pulse voltammetry (DPV), it accurately detects glucose (biomarker) and metformin (drug) concentrations in ISF. Validation experiments *in vivo* have demonstrated that the MCBM system exhibits high sensitivity, specificity, and biocompatibility, enabling wireless real-time data analysis and feedback *via* a smartphone app. Its dual POCT capability of simultaneous drug/biomarker detection will provide great potential for dynamic pharmacokinetic/pharmacodynamic monitoring for diabetic patients, supporting personalized medication adjustments. This advances precision medicine with real-time dosage optimization depending on collaborative monitoring of biomarkers, facilitating safe and effective individualized diabetes treatment.

5. Prospects and challenges of MN-based electrochemical biosensors

MN-based electrochemical biosensors have emerged as a more transformative platform for minimally invasive biosensing when compared with traditional biosensors and conventional blood testing. By leveraging minimally invasive sampling of interstitial fluid, user-friendly operation, and rapid analysis, MN-based electrochemical biosensors enable effective long-term monitoring, opening a promising platform for decentralized diagnostics. Such attributes support their wide application across diverse fields, ranging from chronic disease management to cancer and infection diagnosis, therapeutic drug monitoring and sports physiology tracking.

Based on these advantages, the prospects of MN-based electrochemical biosensors include the following: (1) enhanced analytical performance by integrating cutting-edge technologies. For instance, nanomaterials such as gold nanoflowers and graphene nanosheets can expand the sensing surface area and enhance signal amplification, thereby improving the detection sensitivity for trace biomarkers. Microfabrication techniques, including 3D printing and lithography, enable precise optimization of MN geometry and array design, facilitating device miniaturization, integration, and scalable production. CRISPR technology enhances the specificity of nucleic acid detection, allowing accurate identification of viral nucleic acids or tumor-derived cell-free DNA for early disease screening. (2) Broad monitoring scope in patient populations and multiplexed testing. MN-based electrochemical biosensors enable real-time continuous monitoring over multiple days, replacing discrete measurements, and are particularly well-suited for vulnerable populations, including children, the elderly, and patients with needle phobia. Notably, the integration of multiplex testing strategies (*e.g.*, spatial encoding, signal differentiation, multi-target recognition elements) allows simultaneous quantification of multiple biomarkers (*e.g.*, metabolites, proteins, nucleic acids) in ISF. This design directly broadens the analytical scope for biomarker coverage while extending accessibility to diverse patient groups, thereby enhancing the clinical utility for comprehensive health assessment. (3) Diversified practical application scenarios. MN-based electrochemical biosensors will be further highlighted in critical scenarios (*e.g.*, home healthcare and emergency care). In home settings, miniaturized and wearable devices can connect with smartphones or internet-of-things (IoT) tools for real-time data transmission and remote consultation, enabling self-monitoring of health indicators (*e.g.*, glucose, uric acid) without hospital visits. In emergency care, their rapid response allows quick detection of cardiac markers (*e.g.*, troponin) or infection factors (*e.g.*, procalcitonin), helping clinicians make timely treatment decisions. Collectively, MN-based electrochemical biosensors hold great promise for revolutionizing personalized diagnostics, decentralized healthcare, and public health surveillance.

To achieve these goals, several challenges associated with MN-based electrochemical biosensors should be addressed: (1) the integration of electrochemical sensing components (*e.g.*, working, reference, counter electrodes) into microneedle structures faces miniaturization and stability dilemmas.[159,160] Reducing electrode size to fit microneedle dimensions often leads to decreased electrochemically active area, resulting in low current signals, poor signal-to-noise ratio, and limited sensitivity for detecting low-abundance biomarkers in interstitial fluid. (2) The interface compatibility between microneedle substrates (*e.g.*, polymers, metals, hydrogels) and sensing materials (*e.g.*, conductive nanomaterials, enzymes, antibodies, aptamers) is insufficient.[161–163] Microneedles may bend, break, or deform during insertion, damaging the sensing layer and causing irreversible performance loss. Sensing layers are prone to delamination, degradation, or activity loss during skin penetration and prolonged contact with biological fluids, undermining sensing reproducibility and long-term reliability. (3) Fluid dynamics (mass transfer)

limitations within microneedle modules affect electrochemical reaction efficiency.[164] The confined space of microneedle channels or porous structures restricts the diffusion of analytes, electrolytes, and reaction products, leading to slow response kinetics and inaccurate quantification. (4) Interference from complex ISF components (*e.g.*, proteins, small molecules, ions) is amplified in MN-based electrochemical detection.[165,166] The lack of effective *in situ* anti-interference designs within microneedle modules leads to false signals and reduced detection specificity. (5) Calibrating sensor response for individual variations in skin physiology and ISF composition remains challenging, as current MN-based biosensing modules lack real-time self-calibration capabilities.[167,168] Furthermore, individual variations in skin anatomy, dynamic changes in interstitial fluid pressure, and local tissue responses pose substantial obstacles to obtaining consistent and reproducible results across diverse populations, necessitating the development of robust calibration strategies. Overcoming the challenges of transforming continuous data streams into clinically actionable insights and establishing clear regulatory pathways for integrated medical devices represents crucial steps toward successful commercialization and widespread adoption. To keep pace with monitoring issues of global health promptly, MN-based electrochemical biosensors should be gradually translated into clinical practice and adapted to market demands. In particular, their integration with IoT and artificial intelligence algorithms will fundamentally transform healthcare delivery, enabling predictive and personalized medicine through real-time data acquisition and intelligent analysis.

Author contributions

RQY: conceptualization, methodology, formal analysis, writing – original draft, and writing – review & editing. XXM: conceptualization, methodology, formal analysis and writing – review & editing. GDZ: conceptualization and formal analysis. GHZ: methodology and formal analysis. WL: methodology and formal analysis. JL: conceptualization. YXX: formal analysis and investigation. SS: conceptualization, methodology, formal analysis, and writing – review & editing. LLW: conceptualization, methodology, formal analysis, resources and writing – review & editing.

Conflicts of interest

There are no conflicts to declare.

Data availability

No primary research results, software or code have been involved and no new data were generated or analyzed as part of this review.

Acknowledgements

This review is supported by the Basic Research Program of Jiangsu (Grant No. BK20253006), the Basic Research Program of Jiangsu (Grant No. BK20243057), the National Natural Science Foundation of China (Grant No. 62235008), the Basic Research Program of Jiangsu (Grant No. BK20230364), the Open Research Fund of State Key Laboratory of Digital Medical Engineering (Grant No. 2025-M09) and the Postgraduate Research & Practice Innovation Program of Jiangsu Province (Grant No. KYCX25_1212).

References

1 J. Kim, A. S. Campbell, B. E.-F. De Ávila and J. Wang, *Nat. Biotechnol.*, 2019, **37**, 389–406.
2 H. Duan, S. Peng, S. He, S.-Y. Tang, K. Goda, C. H. Wang and M. Li, *Adv. Sci.*, 2025, **12**, 2411433.
3 K. Mahato, T. Saha, S. Ding, S. S. Sandhu, A.-Y. Chang and J. Wang, *Nat. Electron.*, 2024, **7**, 735–750.
4 J. Madden, C. O'mahony, M. Thompson, A. O'riordan and P. Galvin, *Sens. Bio-Sens. Res.*, 2020, **29**, 100348.
5 S. Ma, J. Li, L. Pei, N. Feng and Y. Zhang, *J. Pharm. Anal.*, 2023, **13**, 111–126.
6 M. Friedel, I. A. P. Thompson, G. Kasting, R. Polsky, D. Cunningham, H. T. Soh and J. Heikenfeld, *Nat. Biomed. Eng.*, 2023, **7**, 1541–1555.
7 F. Tasca, C. Tortolini, P. Bollella and R. Antiochia, *Curr. Opin. Electrochem.*, 2019, **16**, 42–49.
8 P. D. Thungon, A. Kakoti, L. Ngashangva and P. Goswami, *Biosens. Bioelectron.*, 2017, **97**, 83–99.
9 L. K. Vora, A. H. Sabri, P. E. Mckenna, A. Himawan, A. R. J. Hutton, U. Detamornrat, A. J. Paredes, E. Larrañeta and R. F. Donnelly, *Nat. Rev. Bioeng.*, 2024, **2**, 64–81.
10 A. H. Hung, N. U. Kamat, A. Bermudez, S. M. Boczek, F. J. Garcia-Marqués, Y. L. Tan, J. Hwang, P. D. Sinawang, D. Ilyin, G. B. Jacobson, U. Demirci, S. P. Poplack, S. J. Pitteri and J. M. Desimone, *Sci. Adv.*, 2025, **11**, eadx5492.
11 N. U. Rajesh, J. Hwang, Y. Xu, M. A. Saccone, A. H. Hung, R. A. S. Hernandez, I. A. Coates, M. M. Driskill, M. T. Dulay, G. B. Jacobson, S. Tian, J. L. Perry and J. M. Desimone, *Adv. Mater.*, 2024, **36**, 2404606.
12 H. Zhang, H. Zhao, X. Zhao, C. Xu, D. Franklin, A. Vázquez-Guardado, W. Bai, J. Zhao, K. Li, G. Monti, W. Lu, A. Kobeissi, L. Tian, X. Ning, X. Yu, S. Mehta, D. Chanda, Y. Huang, S. Xu, B. E. P. White and J. A. Rogers, *Adv. Funct. Mater.*, 2021, **31**, 2100576.
13 Y. Wang, L. Cai, L. Fan, L. Wang, F. Bian, W. Sun and Y. Zhao, *Adv. Sci.*, 2025, **12**, 2409519.
14 Z. Le, J. Yu, Y. J. Quek, B. Bai, X. Li, Y. Shou, B. Myint, C. Xu and A. Tay, *Mater. Today*, 2023, **63**, 137–169.
15 H. Abdullah, T. Phairatana and I. Jeerapan, *Microchim. Acta*, 2022, **189**, 440.

16 X. Zhou, S. Huang, D. Zhang, W. Liu, W. Gao, Y. Xue and L. Shang, *Anal. Chem.*, 2023, **95**, 12104–12112.
17 Z. Bao, S. Lu, D. Zhang, G. Wang, X. Cui and G. Liu, *Adv. Healthcare Mater.*, 2024, **13**, 2303511.
18 R. Mei, Y. Wang, S. Shi, X. Zhao, Z. Zhang, X. Wang, D. Shen, Q. Kang and L. Chen, *Anal. Chem.*, 2022, **94**, 16069–16078.
19 H. Sun, Y. Zheng, G. Shi, H. Haick and M. Zhang, *Small*, 2023, **19**, 2207539.
20 G.-S. Liu, Y. Kong, Y. Wang, Y. Luo, X. Fan, X. Xie, B.-R. Yang and M. X. Wu, *Biomaterials*, 2020, **232**, 119740.
21 Y. Hu, E. Chatzilakou, Z. Pan, G. Traverso and A. K. Yetisen, *Adv. Sci.*, 2024, **11**, 2306560.
22 S. Samavat, J. Lloyd, L. O'dea, W. Zhang, E. Preedy, S. Luzio and K. S. Teng, *Biosens. Bioelectron.*, 2018, **118**, 224–230.
23 I. Eş, A. Kafadenk, M. B. Gormus and F. Inci, *Small*, 2023, **19**, 2206510.
24 M. Parrilla, N. Claes, C. Toyos-Rodríguez, C. E. M. K. Dricot, A. Steijlen, S. Lebeer, S. Bals and K. De Wael, *Biosens. Bioelectron.*, 2025, **289**, 117934.
25 M. Parrilla, A. Steijlen, R. Kerremans, J. Jacobs, L. Den Haan, J. De Vreese, Y. V. Géron, P. Clerx, R. Watts and K. De Wael, *Chem. Eng. J.*, 2024, **500**, 157254.
26 A. Keirouz, Y. L. Mustafa, J. G. Turner, E. Lay, U. Jungwirth, F. Marken and H. S. Leese, *Small*, 2023, **19**, 2206301.
27 P. W. R. Ananda, D. Elim, H. S. Zaman, W. Muslimin, M. G. R. Tunggeng and A. D. Permana, *Int. J. Pharm.*, 2021, **609**, 121204.
28 A. M. N. Fitri, U. Mahfufah, S. B. A. Aziz, N. A. F. Sultan, M. A. S. B. Mahfud, M. D. Saputra, D. Elim, N. F. Bakri, A. Arjuna, Y. W. Sari, J. Domínguez-Robles, B. Pamornpathomkul, M. Mir and A. D. Permana, *Int. J. Pharm.*, 2024, **660**, 124307.
29 S. Kang, J. E. Song, S.-H. Jun, S.-G. Park and N.-G. Kang, *Pharmaceutics*, 2022, **14**, 1758.
30 Y.-C. Kim, J.-H. Park and M. R. Prausnitz, *Adv. Drug Delivery Rev.*, 2012, **64**, 1547–1568.
31 T. Abbasiasl, S. Sarıca, U. C. Yener, E. Yilgor, I. Yilgor, H. C. Koydemir, E. Öztürk and L. Beker, *Adv. Mater. Technol.*, 2025, **10**, e00891.
32 Y. Cheng, X. Gong, J. Yang, G. Zheng, Y. Zheng, Y. Li, Y. Xu, G. Nie, X. Xie, M. Chen, C. Yi and L. Jiang, *Biosens. Bioelectron.*, 2022, **203**, 114026.
33 A. Jaiswar, U. U. Bhamare, G. S. N. K. Rao and M. B. Palkar, *Microchem. J.*, 2025, **218**, 115311.
34 Y. Cheng, X. Luan, J. Weng, L. Zhang and F. Ye, *Chem. Eng. J.*, 2024, **499**, 156130.
35 T. M. Blicharz, P. Gong, B. M. Bunner, L. L. Chu, K. M. Leonard, J. A. Wakefield, R. E. Williams, M. Dadgar, C. A. Tagliabue, R. El Khaja, S. L. Marlin, R. Haghgooie, S. P. Davis, D. E. Chickering and H. Bernstein, *Nat. Biomed. Eng.*, 2018, **2**, 151–157.
36 P. Dardano, I. Rea and L. De Stefano, *Curr. Opin. Electrochem.*, 2019, **17**, 121–127.
37 Á. Cárcamo-Martínez, B. Mallon, J. Domínguez-Robles, L. K. Vora, Q. K. Anjani and R. F. Donnelly, *Int. J. Pharm.*, 2021, **599**, 120455.
38 L. Niu, L. Y. Chu, S. A. Burton, K. J. Hansen and J. Panyam, *J. Controlled Release*, 2019, **294**, 268–278.
39 Z. F. Rad, R. E. Nordon, C. J. Anthony, L. Bilston, P. D. Prewett, J.-Y. Arns, C. H. Arns, L. Zhang and G. J. Davies, *Microsyst. Nanoeng.*, 2017, **3**, 17034.
40 K. Lee and H. Jung, *Biomaterials*, 2012, **33**, 7309–7326.
41 J. G. Turner, E. Lay, U. Jungwirth, V. Varenko, H. S. Gill, P. Estrela and H. S. Leese, *Adv. Mater. Technol.*, 2023, **8**, 2300259.
42 N. U. Rajesh, I. Coates, M. M. Driskill, M. T. Dulay, K. Hsiao, D. Ilyin, G. B. Jacobson, J. W. Kwak, M. Lawrence, J. Perry, C. O. Shea, S. Tian and J. M. Desimone, *JACS Au*, 2022, **2**, 2426–2445.
43 I. Atay, E. Yilgör, G. Neşer, T. Abbasiasl, M. B. Yagci, I. Yilgör and L. Beker, *Adv. Mater. Interfaces*, 2025, **12**, 2500001.
44 S. Babity, M. Roohnikan and D. Brambilla, *Small*, 2018, **14**, 1803186.
45 L. Bao, J. Park, G. Bonfante and B. Kim, *Drug Delivery Transl. Res.*, 2022, **12**, 395–414.
46 Y. T. He, L. Liang, Z. Q. Zhao, L. F. Hu, W. M. Fei, B. Z. Chen, Y. Cui and X. D. Guo, *J. Drug Delivery Sci. Technol.*, 2022, **74**, 103518.
47 L. Liu, H. Kai, K. Nagamine, Y. Ogawa and M. Nishizawa, *RSC Adv.*, 2016, **6**, 48630–48635.
48 E. M. Eltayib, *RSC Adv.*, 2025, **15**, 18697–18714.
49 X. Wang, K. Li, X. Li, S. Wu, Z. Lv, L. Guan, J. Cheng and H. Wang, *Biosens. Bioelectron.*, 2025, **287**, 117701.
50 H. Kai and A. Kumatani, *JPhys Energy*, 2021, **3**, 024006.
51 R. He, Y. Niu, Z. Li, A. Li, H. Yang, F. Xu and F. Li, *Adv. Healthcare Mater.*, 2020, **9**, 1901201.
52 L. Barnum, J. Quint, H. Derakhshandeh, M. Samandari, F. Aghabaglou, A. Farzin, L. Abbasi, S. Bencherif, A. Memic, P. Mostafalu and A. Tamayol, *Adv. Healthcare Mater.*, 2021, **10**, 2001922.
53 M. Zheng, Z. Wang, H. Chang, L. Wang, S. W. T. Chew, D. C. S. Lio, M. Cui, L. Liu, B. C. K. Tee and C. Xu, *Adv. Healthcare Mater.*, 2020, **9**, 1901683.
54 J. G. Turner, L. R. White, P. Estrela and H. S. Leese, *Macromol. Biosci.*, 2021, **21**, 2170003.
55 I. R. Ausri, S. Sadeghzadeh, S. Biswas, H. Zheng, P. Ghavaminejad, M. D. T. Huynh, F. Keyvani, E. Shirzadi, F. A. Rahman, J. Quadrilatero, A. Ghavaminejad and M. Poudineh, *Adv. Mater.*, 2024, **36**, 2470256.
56 W. Park, S.-W. Maeng, J. W. Mok, M. Choi, H. J. Cha, C.-K. Joo and S. K. Hahn, *Biomacromolecules*, 2023, **24**, 1445–1452.
57 J. Zhao, J. Lv, G. Ling and P. Zhang, *Int. J. Biol. Macromol.*, 2024, **254**, 127745.
58 J. Zhang, Y. Zheng, J. Lee, A. Hoover, S. A. King, L. Chen, J. Zhao, Q. Lin, C. Yu, L. Zhu and X. Wu, *Adv. Sci.*, 2023, **10**, 2203943.
59 Z. Guo, H. Liu, Z. Shi, L. Lin, Y. Li, M. Wang, G. Pan, Y. Lei and L. Xue, *J. Mater. Chem. B*, 2022, **10**, 3501–3511.

60 X. Xu, B. Bai, C. Ding, H. Wang and Y. Suo, *Ind. Eng. Chem. Res.*, 2015, **54**, 3268–3278.
61 T. D. Naylor, *Compr. Polym. Sci.*, 1989, **2**, 643–668.
62 K. Alharbi, A. Ghoneim, A. Ebid, H. El-Hamshary and M. H. El-Newehy, *Int. J. Biol. Macromol.*, 2018, **116**, 224–231.
63 M. Niazi, E. Alizadeh, A. Zarebkohan, K. Seidi, M. H. Ayoubi-Joshaghani, M. Azizi, H. Dadashi, H. Mahmudi, T. Javaheri, M. Jaymand, M. R. Hamblin, R. Jahanban-Esfahlan and Z. Amoozgar, *Adv. Funct. Mater.*, 2021, **31**, 2104123.
64 M. Saidi, A. Dabbaghi and S. Rahmani, *Polym. Bull.*, 2020, **77**, 3989–4010.
65 S. Panpinit, S.-A. Pongsomboon, T. Keawin and S. Saengsuwan, *React. Funct. Polym.*, 2020, **156**, 104739.
66 S. Yao, C. Zhang, J. Ping and Y. Ying, *Biosens. Bioelectron.*, 2024, **250**, 116066.
67 J. Wang, Y. Liu, C. Yu, X. Wang and J. Wang, *J. Hazard. Mater.*, 2024, **470**, 134216.
68 A. F. Aroche, H. E. Nissan and M. A. Daniele, *Adv. Healthcare Mater.*, 2025, **14**, 2401782.
69 H. Han, D. Pan, F. Pan, X. Hu and R. Zhu, *Sens. Actuators, B*, 2021, **327**, 128883.
70 E. Skaria, B. A. Patel, M. S. Flint and K. W. Ng, *Anal. Chem.*, 2019, **91**, 4436–4443.
71 J. Shen, W. Fu, W. Wei, C. Qian, G. Ni and D. Zhu, *Biosens. Bioelectron.*, 2025, **280**, 117426.
72 E. Fakeih, S. S. Shetty, W. Hanif, K. Mutabagani, K. N. Salama and D. Alsulaiman, *ACS Mater. Lett.*, 2025, **7**, 3595–3603.
73 Z. Li, Y. Wang, R. Zhang, Z. Liu, Z. Chang, Y. Deng and X. Qi, *ACS Nano*, 2024, **18**, 23876–23893.
74 R. Yao, Z. Wu, O. Y. Olatunji, K. E. Yunusov, F. M. U. Turakulov, J. Chen and G. Jiang, *Microchem. J.*, 2025, **219**, 115991.
75 F. Rahman, A. Ryan, A. Bocchino, P. Galvin and S. R. Teixeira, *Sens. Bio-Sens. Res.*, 2025, **48**, 100777.
76 A. Caliò, P. Dardano, V. Di Palma, M. F. Bevilacqua, A. Di Matteo, H. Iuele and L. De Stefano, *Sens. Actuators, B*, 2016, **236**, 343–349.
77 P. R. Miller, R. M. Taylor, B. Q. Tran, G. Boyd, T. Glaros, V. H. Chavez, R. Krishnakumar, A. Sinha, K. Poorey, K. P. Williams, S. S. Branda, J. T. Baca and R. Polsky, *Commun. Biol.*, 2018, **1**, 173.
78 S. Zhou, Y. Chino, T. Kasama, R. Miyake, S. Mitsuzawa, Y. Luan, N. B. Ahmad, H. Hibino and M. Takai, *ACS Nano*, 2024, **18**, 26541–26559.
79 D. Ai, X. Tang, Z. Meng, Y. Yu, X. Guo and Y. Wang, *Anal. Methods*, 2025, **17**, 7541–7550.
80 Y. Liu, Q. Yu, L. Ye, L. Yang and Y. Cui, *Lab Chip*, 2023, **23**, 421–436.
81 Z. Li, W. Sun, Z. Shi, Y. Cao, Y. Wang, D. Lu, M. Jiang, Z. Wang, J. L. Marty and Z. Zhu, *Sens. Actuators, B*, 2025, **422**, 136606.
82 R. Tarpey, S. Islam, B. Bernardo, M. Singh, E. A. Lee, J. M. Karp, Y. Lee, E. T. Roche and W. Ronan, *Smart Mater. Struct.*, 2024, **33**, 125002.
83 P. Liu, H. Du, Y. Chen, H. Wang, J. Mao, L. Zhang, J. Tao and J. Zhu, *J. Mater. Chem. B*, 2020, **8**, 2032–2039.
84 L. Zhou, N. Liang, Y. Zheng, X. Sun, J. He and B. Huang, *Appl. Mater. Today*, 2025, **46**, 102869.
85 Y. Wu, F. Tehrani, H. Teymourian, J. Mack, A. Shaver, M. Reynoso, J. Kavner, N. Huang, A. Furmidge, A. Duvvuri, Y. Nie, L. M. Laffel, F. J. Doyle III, M.-E. Patti, E. Dassau, J. Wang and N. Arroyo-Currás, *Anal. Chem.*, 2022, **94**, 8335–8345.
86 M. Reynoso, A.-Y. Chang, Y. Wu, R. Murray, S. Suresh, Y. Dugas, J. Wang and N. Arroyo-Currás, *Biosens. Bioelectron.*, 2024, **244**, 115802.
87 T. Laochai, J. Yukird, N. Promphet, J. Qin, O. Chailapakul and N. Rodthongkum, *Biosens. Bioelectron.*, 2022, **203**, 114039.
88 G. Karuppaiah, M.-H. Lee, S. Bhansali and P. Manickam, *Biosens. Bioelectron.*, 2023, **239**, 115600.
89 E. L. Vanderlaan, J. K. Nolan, J. Sexton, C. Evans-Molina, H. Lee and S. L. Voytik-Harbin, *Biosens. Bioelectron.*, 2023, **235**, 115409.
90 P. Ghavaminejad, A. Ghavaminejad, H. Zheng, K. Dhingra, M. Samarikhalaj and M. Poudineh, *Adv. Healthcare Mater.*, 2023, **12**, 2202362.
91 G. Zhong, Q. Liu, Q. Wang, H. Qiu, H. Li and T. Xu, *Biosens. Bioelectron.*, 2024, **265**, 116697.
92 A. M. V. Mohan, J. R. Windmiller, R. K. Mishra and J. Wang, *Biosens. Bioelectron.*, 2017, **91**, 574–579.
93 F. Bakhshandeh, H. Zheng, N. G. Barra, S. Sadeghzadeh, I. Ausri, P. Sen, F. Keyvani, F. Rahman, J. Quadrilatero, J. Liu, J. D. Schertzer, L. Soleymani and M. Poudineh, *Adv. Mater.*, 2024, **36**, 2313743.
94 Y. Dai, J. Nolan, E. Madsen, M. Fratus, J. Lee, J. Zhang, J. Lim, S. Hong, M. A. Alam, J. C. Linnes, H. Lee and C. H. Lee, *ACS Appl. Mater. Interfaces*, 2023, **15**, 56760–56773.
95 D. M. E. Freeman, D. K. Ming, R. Wilson, P. L. Herzog, C. Schulz, A. K. G. Felice, Y.-C. Chen, D. O'hare, A. H. Holmes and A. E. G. Cass, *ACS Sens.*, 2023, **8**, 1639–1647.
96 L. Jing, Y. Fan, B. Chen, D. Li, Y. He, G. Zhang, L. Liang, J. Du, Y. Wang and X. Guo, *Chem. Eng. J.*, 2024, **502**, 157488.
97 M. Dervisevic, J. Harberts, R. Sánchez-Salcedo and N. H. Voelcker, *Adv. Mater.*, 2024, **36**, 2412999.
98 Z. Li, F. Chen, N. Zhu, L. Zhang and Z. Xie, *ACS Nano*, 2023, **17**, 21935–21946.
99 M. Parrilla, M. Cuartero, S. P. Sánchez, M. Rajabi, N. Roxhed, F. Niklaus and G. A. Crespo, *Anal. Chem.*, 2019, **91**, 1578–1586.
100 X. Huang, S. Zheng, B. Liang, M. He, F. Wu, J. Yang, H.-J. Chen and X. Xie, *Microsyst. Nanoeng.*, 2023, **9**, 25.
101 M. Dervisevic, E. Dervisevic, L. Esser, C. D. Easton, V. J. Cadarso and N. H. Voelcker, *Biosens. Bioelectron.*, 2023, **222**, 114955.
102 S. Odinotski, K. Dhingra, A. Ghavaminejad, H. Zheng, P. Ghavaminejad, H. Gaouda, D. Mohammadrezaei and M. Poudineh, *Small*, 2022, **18**, 2200201.

103 B. Yang, X. Fang and J. Kong, *Adv. Funct. Mater.*, 2020, **30**, 2000591.
104 B. Yang, J. Kong and X. Fang, *Nat. Commun.*, 2022, **13**, 3999.
105 B. Yang, H. Wang, J. Kong and X. Fang, *Nat. Commun.*, 2024, **15**, 1936.
106 R. Yuan, J. Cai, J. Li, Y. Xu, J. Ma, L. Wang and S. Su, *ACS Sens.*, 2025, **10**, 5684–5693.
107 J. Xu, B. Yang, J. Kong, Y. Zhang and X. Fang, *Adv. Healthcare Mater.*, 2023, **12**, 2203133.
108 N. Poursharifi, M. Hassanpouramiri, A. Zink, M. Ucuncu and O. Parlak, *Adv. Mater.*, 2024, **36**, 2403758.
109 B. Ciui, A. Martin, R. K. Mishra, B. Brunetti, T. Nakagawa, T. J. Dawkins, M. Lyu, C. Cristea, R. Sandulescu and J. Wang, *Adv. Healthcare Mater.*, 2018, **7**, 1701264.
110 M. Dervisevic, M. Alba, T. E. Adams, B. Prieto-Simon and N. H. Voelcker, *Biosens. Bioelectron.*, 2021, **192**, 113496.
111 L. Wang, S.-J. Chang, C.-J. Chen and J.-T. Liu, *Coord. Chem. Rev.*, 2025, **543**, 216907.
112 H. Teymourian, A. Barfidokht and J. Wang, *Chem. Soc. Rev.*, 2020, **49**, 7671–7709.
113 V. Myndrul, E. Coy, N. Babayevska, V. Zahorodna, V. Balitskyi, I. Baginskiy, O. Gogotsi, M. Bechelany, M. T. Giardi and I. Iatsunskyi, *Biosens. Bioelectron.*, 2022, **207**, 114141.
114 G. Rattu, N. Khansili, V. K. Maurya and P. M. Krishna, *Environ. Chem. Lett.*, 2021, **19**, 1135–1152.
115 X. Li, Y. Zhang, L. Xu, A. Wang, Y. Zou, T. Li, L. Huang, W. Chen, S. Liu, K. Jiang, X. Zhang, D. Wang, L. Zhang, Z. Zhang, Z. Zhang, X. Chen, W. Jia, A. Zhao, X. Yan, H. Zhou, L. Zhu, X. Ma, Z. Ju, W. Jia, C. Wang, J. Loscalzo, Y. Yang and Y. Zhao, *Cell Metab.*, 2023, **35**, 200–211.
116 X. Xing, B. Yao, Q. Wu, R. Zhang, L. Yao, J. Xu, G. Gao and W. Chen, *Biosens. Bioelectron.*, 2022, **198**, 113804.
117 Y. Wu, P. Deng, Y. Tian, J. Feng, J. Xiao, J. Li, J. Liu, G. Li and Q. He, *J. Nanobiotechnol.*, 2020, **18**, 112.
118 M. Dervisevic and N. H. Voelcker, *ACS Mater. Lett.*, 2023, **5**, 1851–1858.
119 Y. Zhao, H. Zhang, Y. Li, X. Yu, Y. Cai, X. Sha, S. Wang, Z. Zhan, J. Xu and L. Liu, *Biosens. Bioelectron.*, 2021, **186**, 113291.
120 C. Moccia, M. Cherubini, M. Fortea, A. Akinbote, P. Padmanaban, V. Beltran-Sastre and K. Haase, *Adv. Sci.*, 2023, **10**, 2302561.
121 A. L. Hevener and S. M. Correa, *Nat. Metab.*, 2025, **7**, 1114–1122.
122 W. Tonnus, F. Maremonti, S. Gavali, M. N. Schlecht, F. Gembardt, A. Belavgeni, N. Leinung, K. Flade, N. Bethe, S. Traikov, A. Haag, D. Schilling, S. Penkov, M. Mallais, C. Gaillet, C. Meyer, M. Katebi, A. Ray, L. M. S. Gerhardt, A. Brucker, J. N. Becker, M. Tmava, L. Schlicker, A. Schulze, N. Himmerkus, A. Shevchenko, M. Peitzsch, U. Barayeu, S. Nasi, J. Putz, K. S. Korach, J. Neugarten, L. Golestaneh, C. Hugo, J. U. Becker, J. M. Weinberg, S. Lorenz, B. Proneth, M. Conrad, E. Wolf, B. Plietker, R. Rodriguez, D. A. Pratt, T. P. Dick, M. Fedorova, S. R. Bornstein and A. Linkermann, *Nature*, 2025, **645**, 1011–1019.
123 N. Deubner, D. Berliner, A. Frey, G. Güder, S. Brenner, W. Fenske, B. Allolio, G. Ertl, C. E. Angermann and S. Störk, *Eur. J. Heart Failure*, 2012, **14**, 1147–1154.
124 C. Atila, C. O. Sailer, S. Bassetti, S. Tschudin-Sutter, R. Bingisser, M. Siegemund, S. Osswald, K. Rentsch, M. Rueegg, S. Schaerli, G. M. Kuster, R. Twerenbold and M. Christ-Crain, *Eur. J. Endocrinol.*, 2021, **184**, 409–418.
125 T. Dhondup and Q. Qian, *Blood Purif.*, 2017, **43**, 179–188.
126 A. D. Wickenden, *Pharmacol. Ther.*, 2002, **94**, 157–182.
127 K.-I. Jang, H. N. Jung, J. W. Lee, S. Xu, Y. H. Liu, Y. Ma, J.-W. Jeong, Y. M. Song, J. Kim, B. H. Kim, A. Banks, J. W. Kwak, Y. Yang, D. Shi, Z. Wei, X. Feng, U. Paik, Y. Huang, R. Ghaffari and J. A. Rogers, *Adv. Funct. Mater.*, 2016, **26**, 7281–7290.
128 J. T. Reeder, J. Choi, Y. Xue, P. Gutruf, J. Hanson, M. Liu, T. Ray, A. J. Bandodkar, R. Avila, W. Xia, S. Krishnan, S. Xu, K. Barnes, M. Pahnke, R. Ghaffari, Y. Huang and J. A. Rogers, *Sci. Adv.*, 2019, **5**, eaau6356.
129 G. J. Casimir, N. Lefèvre, F. Corazza, J. Duchateau and M. Chamekh, *Front. Immunol.*, 2018, **9**, 00475.
130 W. Aoi and Y. Marunaka, *BioMed Res. Int.*, 2014, **2014**, 598986.
131 S. R. Madhvapathy, S. Cho, E. Gessaroli, E. Forte, Y. Xiong, L. Gallon and J. A. Rogers, *Nat. Rev. Nephrol.*, 2025, **21**, 443–463.
132 J. J. García-Guzmán, C. Pérez-Ràfols, M. Cuartero and G. A. Crespo, *ACS Sens.*, 2021, **6**, 1129–1137.
133 Y. Marunaka, *World J. Diabetes*, 2015, **6**, 125–135.
134 T. Moniz, S. A. C. Lima and S. Reis, *Carbohydr. Polym.*, 2021, **266**, 118098.
135 M. Cohen and R. Khalaila, *J. Psychosom. Res.*, 2014, **77**, 420–425.
136 H. Wiig and M. A. Swartz, *Physiol. Rev.*, 2012, **92**, 1005–1060.
137 U. N. Wijayaratna, S. D. Kiridena, J. D. Adams, C. J. Behrend and J. N. Anker, *Adv. Funct. Mater.*, 2021, **31**, 2104124.
138 L. Kananen, M. Hurme, A. Bürkle, M. Moreno-Villanueva, J. Bernhardt, F. Debacq-Chainiaux, B. Grubeck-Loebenstein, M. Malavolta, A. Basso, F. Piacenza, S. Collino, E. S. Gonos, E. Sikora, D. Gradinaru, E. H. J. M. Jansen, M. E. T. Dollé, M. Salmon, W. Stuetz, D. Weber, T. Grune, N. Breusing, A. Simm, M. Capri, C. Franceschi, E. Slagboom, D. Talbot, C. Libert, J. Raitanen, S. Koskinen, T. Härkänen, S. Stenholm, M. Ala-Korpela, T. Lehtimäki, O. T. Raitakari, O. Ukkola, M. Kähönen, M. Jylhä and J. Jylhävä, *GeroScience*, 2023, **45**, 85–103.
139 H. Jia and L. Zhang, *Theranostics*, 2025, **15**, 245–257.
140 B. Yang, X. Fang and J. Kong, *ACS Appl. Mater. Interfaces*, 2019, **11**, 38448–38458.
141 A. Dey, S. Kern and I. Skoog, *Alzheimer's Dementia*, 2024, **20**, e086271.
142 M. Li, Z. Wang, T. Ye, T. Wang, J. Li, S. Wang, P. Song, Y.-Y. Song and C. Zhao, *Chem. Eng. J.*, 2025, **519**, 165359.

143 P. M. Ridker, G. A. Figtree, M. V. Moorthy, S. Mora and J. E. Buring, *Eur. Heart J.*, 2026, **43**, 306–314.
144 Z. Gao, Z. Lu, S. Zhao, J. You, J. Wang, S. Gao, W. Zhang, R. Cai, S. Wang, Y. Wu, Z. Wang, J. Li, Y. Bao, Q. Han, Y. Xianyu, J. Yu, Z. Gu and Y. Zhang, *Nano Today*, 2025, **64**, 102777.
145 R. Das, E. Istif, R. Cebecioglu, M. Ali, Y. Atik, Ç. Dağ, E. Celikbas, G. Demirci, F. Acar, M. Hasanreisoğlu and L. Beker, *Adv. Mater. Interfaces*, 2025, **12**, 2400789.
146 Y. Chen, H. Fan, W. Liu, J. Wang, T. Wang, R. Yang, L. Zhang, L. Shang and D. Wen, *Adv. Mater.*, 2026, **38**, e14242.
147 H. Zargartalebi, S. Mirzaie, A. Ghavaminejad, S. U. Ahmed, F. Esmaeili, A. Geraili, C. D. Flynn, D. Chang, J. Das, A. Abdrabou, E. H. Sargent and S. O. Kelley, *Science*, 2024, **386**, 1146–1153.
148 X.-W. Chen, Y.-S. Chen, X.-M. Ding, L. Wang, J. Liu and R.-F. Wang, *Tungsten*, 2023, **5**, 81–90.
149 H. Ao, Z. Qian, Y. Zhu, M. Zhao, C. Tang, Y. Huang, H. Feng and A. Wang, *Biosens. Bioelectron.*, 2016, **86**, 542–547.
150 Y. Nedellec, C. Gondran, K. Gorgy, S. Mc Murtry, P. Agostini, O. Elmazria and S. Cosnier, *Biosens. Bioelectron.*, 2021, **180**, 113137.
151 S. Krishnamurthy, S. A. Jazowski, M. L. Roberson, K. Reeder-Hayes, J. J. Tang, S. B. Dusetzina and U. R. Essien, *JAMA Netw. Open*, 2025, **8**, e258086.
152 M. V. Dieci, G. Bisagni, S. Bartolini, A. Schirone, L. Cavanna, A. Musolino, F. Giotta, A. Rimanti, O. Garrone, E. Bertone, K. Cagossi, S. Sarti, A. Ferro, F. Piacentini, E. Orvieto, M. Sanders, F. Miglietta, D. Massa, S. Balduzzi, P. Conte, R. D'amico and V. Guarneri, *JAMA Oncol.*, 2025, **11**, 386–393.
153 X. Sun, G. Zhong, Y. Zeng, T. Xu and Y. Liu, *Anal. Chem.*, 2025, **97**, 15941–15948.
154 Y. Liu, J. Liu, Y. Chen, G. Zhang, Q. Wang and Y. Li, *Anal. Chem.*, 2025, **97**, 1539–1545.
155 M. Qi, W. Fu, X. Ying, B. Zhu, Z. Zhao, L. Zhou, W. Li and B. Su, *Anal. Chem.*, 2025, **97**, 10638–10645.
156 X. Li, S. Zheng, M. He, X. Huang, C. Yang, J. Mo, J. Yang, C. Yang, H. Chen and X. Xie, *Innovation*, 2025, **6**, 100781.
157 A.-Y. Chang, M. Lin, L. Yin, M. Reynoso, S. Ding, R. Liu, Y. Dugas, A. Casanova, G. Park, Z. Li, H. Luan, N. Askarinam, F. Zhang, S. Xu and J. Wang, *Nat. Biomed. Eng.*, 2026, **10**, 94–109.
158 J. Yang, X. Gong, Y. Zheng, H. Duan, S. Chen, T. Wu, C. Yi, L. Jiang and H. Haick, *Nat. Commun.*, 2025, **16**, 6260.
159 Q. Huang, X. Lin, D. Nie, J. Wang, K. Fan, Z. Zhao and Z. Han, *Adv. Funct. Mater.*, 2025, **35**, 2503027.
160 Y. Liu, L. Yang and Y. Cui, *Microsyst. Nanoeng.*, 2024, **10**, 112.
161 A. Barhoum, O. Sadak, I. A. Ramirez and N. Iverson, *Adv. Colloid Interface Sci.*, 2023, **317**, 102920.
162 W.-Y. Guo and M.-G. Ma, *J. Mater. Chem. A*, 2024, **12**, 9371–9399.
163 H. Li and R. F. Donnelly, *Matter*, 2024, **7**, 2663–2664.
164 P.-J. Chiang, X.-J. Lin, S.-J. Shin, Y.-C. Weng, H.-M. Chen, Y.-T. Wu, Y.-Y. Chen, H.-R. Chen, L.-H. Chen and T.-C. Liu, *Sens. Actuators, B*, 2026, **449**, 139056.
165 J. Liu, J. Liu, Y. Liang, J. Yang, Y. Lin and Y. Li, *Anal. Chem.*, 2025, **97**, 373–381.
166 H. Teymourian, F. Tehrani, K. Mahato and J. Wang, *Adv. Healthcare Mater.*, 2021, **10**, 2002255.
167 O. Heifler, E. Borberg, N. Harpak, M. Zverzhinetsky, V. Krivitsky, I. Gabriel, V. Fourman, D. Sherman and F. Patolsky, *ACS Nano*, 2021, **15**, 12019–12033.
168 B. Zhu, L. Zhu, X. Li, Z. Zhao, J. Cao, M. Qi, Z. Gao, L. Zhou and B. Su, *Research*, 2024, **7**, 0508.